

Polarization Effects in γ P Gravitational Scattering with Applications to Dark Matter

Calev Isaacson

MSc by Research

University of York
Physics, Engineering, and Technology
January 2023

Abstract

Using a simple perturbative approach to quantum gravity, we consider gravitational scattering of high-energy, polarized photons on a massive scalar target. We find that due to the exchange of virtual gravitons, there is a non-trivial polarization dependence in the photon scattering behavior, not previously considered in the literature. Our results are considered in analogy with scattering in quantum electrodynamics. We find that the polarization dependence in a gravitational field is extremely weak relative to electromagnetic effects. A variety of possible experimental parameters were considered in order to isolate the quantum gravity effects.

Using Monte-Carlo methods, this work models the gravitational scattering of galactic photons in the Dark Matter Halo of the Milky Way. The likelihood of detecting these scattered photons on Earth is then calculated, along with the degree of gravity-induced polarization. Detection of this polarization would provide convincing evidence of the quantum effects of gravity and indirect proof of graviton exchange. Our results indicate that Dark Matter can be thought as polarizing, even in scalar models where Dark Matter only interacts gravitationally. Results also suggest a new method of bounding the mass of the Dark Matter particle from above. Dark Matter was chosen as the scattering target to mitigate interfering non-gravitational effects.

We also briefly discuss polarization effects of photon-scalar scattering as an entanglement breaking channel for maximally entangled photons produced by pair annihilation, which is a fascinating avenue for future research.

Acknowledgements

BS"D

This work could never have taken place without the unwavering guidance of Mikhail Bashkanov and Dan Watts. Thank you for welcoming me to the University of York community and for opening doors into the world of physics research. Our conversations, on topics ranging from Feynman Diagrams to Dark Matter to Monte-Carlo methods, have been a trusted beacon and life-saver during this research.

I would also like to thank Pietro Caradonna for enlightening discussions about photons, polarization, and entanglement. Thank you for being there throughout our long strings of emails!

I also thank Bernard Kay for his incredible insight on the theory-side of things. Having a math professor to consult truly enhanced the quality of the research!

And a special thank you goes to Yvette Fuentes; thank you for your investment of time in our discussions about QFT in curved space-time and entanglement breaking.

Finally, I want to thank my parents and amazing sister who supported my study and allowed me to bounce physics ideas around the home!

Declaration

I declare that this thesis is a presentation of original work and I am the sole author. This work has not previously been presented for an award at this, or any other, University. All sources are acknowledged as References.

Table of contents

| | |
|--|-----------|
| Abstract | 3 |
| Acknowledgements | 5 |
| Declaration | 7 |
| List of figures | 13 |
| List of tables | 15 |
| Nomenclature | 17 |
| 1 Introduction | 19 |
| 1.1 History and Motivation | 19 |
| 1.1.1 Search for Quantum Gravity | 20 |
| 1.1.2 Search for Dark Matter | 21 |
| 1.2 Research Aims | 21 |
| 1.3 Structure of Thesis | 22 |
| 2 Theoretical Background | 25 |
| 2.1 Perturbative Quantum Gravity | 25 |
| 2.2 Deriving the Graviton Propogator | 26 |
| 2.3 Scattering Fundamentals | 29 |
| 3 Scattering Machinery | 31 |
| 3.1 Photon-Scalar Scattering | 31 |
| 3.1.1 Scattering Kinematics | 33 |

Table of contents

| | | |
|----------|---|-----------|
| 3.1.2 | Photon Polarization | 33 |
| 3.2 | Polarization Effects | 35 |
| 3.2.1 | Differential Cross Section | 38 |
| 3.2.2 | Unpolarized Photons | 38 |
| 3.2.3 | Total Cross Sections | 39 |
| 3.2.4 | Likelihood of Scattering | 40 |
| 4 | Gravitational Polarization by Dark Matter | 43 |
| 4.1 | Galactic Halo | 44 |
| 4.1.1 | On the Dark Matter Particle Mass | 45 |
| 4.2 | Monte Carlo Simulation | 46 |
| 4.2.1 | Geometry | 47 |
| 4.3 | Computational Results | 49 |
| 5 | Applications | 53 |
| 5.1 | Additional Considerations | 53 |
| 5.2 | Scattering on Macroscopic Targets | 54 |
| 5.2.1 | Range of Applicability | 55 |
| 5.3 | On the Subject of Entanglement | 56 |
| 6 | Analysis | 59 |
| 6.1 | Polarization Effects of Photon Scattering | 59 |
| 6.2 | Additional Applications | 60 |
| 7 | Conclusions | 61 |
| 7.1 | Discussion | 61 |
| 7.1.1 | Impact on Quantum Gravity | 61 |
| 7.1.2 | Impact of Dark Matter Research | 61 |
| 7.1.3 | Entanglement Breaking | 62 |
| | Appendix A Conventions | 67 |
| | Appendix B Parellel with Electromagentsim | 73 |

| | |
|--|-----------|
| Appendix C Form Factors | 81 |
| Appendix D Additional Monte-Carlo Tests and Results | 83 |

List of figures

| | | |
|-----|---|----|
| 3.1 | Photon-Scalar Scattering via graviton exchange (left) and Electron-Muon Scattering via photon exchange (right). | 31 |
| 3.2 | Rotation of polarization basis vector in the scattering plane. | 35 |
| 3.3 | Rotation of polarization basis vector which is orthogonal to the scattering plane. | 35 |
| 3.4 | Shape of differential cross section as a function of scattering angle θ (averaged over all azimuthal angles ϕ). Blue and Red curves correspond to initial polarization e^\perp and e^\parallel respectively for a 511 KeV photon scattering off a scalar particle. | 39 |
| 3.5 | Shape of unpolarized cross section, where red and blue curves correspond to our results for unpolarized photons given in Eq. 3.15 and the analogous results of Ref. [23] in Eq. 3.16, respectively. | 40 |
| 4.1 | Example of Central Cusp (blue) and Cored Halo (red) density profiles: Navarro-Frenk-White and Isothermal profiles respectively [21]. Dotted line indicates location of Earth on these normalized axes. | 44 |
| 4.2 | Visualization of the emission and scattering of photon relative to the galactic center and Earth. | 48 |
| 4.3 | Each ‘hit’ on the histograms represents the final location of an appropriately scattered photon in an imaginary plane centered around Earth. Each histogram records photons of particular linear polarization. | 49 |
| 4.4 | Each ‘hit’ on the histograms represents the final location of an appropriately scattered photon in an imaginary plane centered around Earth. Results here are reported in number of hits per unit area. Each histogram records photons of particular linear polarization. | 50 |

List of figures

| | | |
|-----|--|----|
| 4.5 | Each ‘hit’ on the above histogram represents the difference between the number of scattered photons of each polarizations at various points on an imaginary plane centered around Earth. | 50 |
| 4.6 | Scattering events vs radius. 10 million photons, log plot. | 51 |
| 4.7 | Scattering events vs radius with normalized NFW density profile (orange line). 1 million photons, log plot. | 51 |
| 5.1 | Cross Section for large angle scattering vs mass energy of target, in double log scale. Red and blue curves correspond to photons of each of the two linear polarization states | 54 |
| D.1 | Photon hits near Earth (a) and (b) correspond to the two states of linear polarization. . | 87 |
| D.2 | Difference between photon hits of either polarization per unit area. | 88 |
| D.3 | Difference between photon hits of either polarization. | 88 |

List of tables

| | | |
|-----|--|----|
| 4.1 | Parameters of Dark Matter Halo | 45 |
| 5.1 | Cross Sections for Typical Bending Angles (according to GR). | 55 |
| 5.2 | Cross Sections for Large Bending Angles. | 55 |
| D.1 | Geometry Tests for Emission and Scattering Angles | 84 |
| D.2 | Geometry Tests for Emission and Scattering Angles Cont'd | 85 |
| D.3 | Geometry Tests for Emission and Scattering Angles Cont'd | 86 |
| D.4 | Geometry Tests for Emission and Scattering Angles Cont'd | 87 |

Nomenclature

Roman Symbols

$D_{\mu\nu,\lambda\sigma}(k)$ Graviton Propagator

$F^{\mu\nu}$ Electromagnetic tensor

G Newton's Gravitational Constant $6.674 \times 10^{-11} \text{m}^3 \text{kg}^{-1} \text{s}^{-2}$

$g^{\mu\nu}$ Curved Metric Tensor

k or K Momentum (massless particle)

\mathcal{L} Lagrangian

L Luminosity

O Order

p or P Momentum (massive particles)

$T^{\mu\nu}$ Stress-energy tensor

Greek Symbols

Φ Photon Flux

ρ_m Mass Density

ρ_t Number Density

$\eta^{\mu\nu}$ Minkowski Metric Tensor

Ω Total Angle

Nomenclature

ϕ Azimuthal Angle

π 3.14...

σ Cross Section

θ Polar Angle

Acronyms / Abbreviations

GR General Relativity

MACHO Massive Compact Halo Object

MC Monte-Carlo

PQG Perturbative Quantum Gravity

WIMP Weakly Interacting Massive Particle

Chapter 1

Introduction

1.1 History and Motivation

Since the rise of quantum mechanics in the 20th century, physicists have devised new models and theories, which describe quantum effects of the fundamental forces of nature [1]. Over several decades, a quantum theory of electromagnetism, known as Quantum Electrodynamics (QED) was slowly developed [2]. In the years which followed, the Weak nuclear force was brought under this umbrella through Electroweak Theory [3]. This was paralleled by the simultaneous development of Quantum Chromodynamics, which describes the Strong force [4]. By the end of the century, the last force of nature, which had no quantum description, was Gravity, arguably the universe's most enigmatic force [1, 5].

Once Einstein's General Relativity (GR) replaced Newtonian gravity in 1905, our understanding of gravity had greatly improved [6]. However, as the century progressed, it soon became evident that this understanding was still incomplete. Specifically, GR is incapable of describing relativistic phenomena where quantum effects become non-trivial, such as inside very strong gravitational fields, or at energies greater than 10^{19} GeV [5]. These limitations preclude detailed description of phenomena such as the very early universe and the space-time near a singularity. A fuller understanding of gravity was therefore desired, and quickly became an area of modern research.

However, there exist major differences between GR and quantum theories. GR is an entirely classical theory which is, roughly speaking, deterministic. One can predict the future of a system with absolute certainty, given enough information about the system. Consider for example, the motion of a body according to field equations of GR, as in Ref. [6]. In contrast, quantum mechanics predicts that

the evolution of states is governed by probabilities, and hence the universe is entirely non-deterministic (for a review, see textbook such as Ref. [7]). As Niels Bohr once wrote "One does not get an answer to the question 'what is the state after collision' but only to the question 'how probable is a given effect of the collision'" [8].

These fundamental, and almost-philosophical differences fueled several famous arguments between Einstein and the founders of quantum theory [8]. For most common purposes, these differences have little practical relevance, due to the distinct range of applicability of each theory. GR is a theory governing 'macroscopic phenomena' with large masses and over large distances, whereas quantum mechanics typically governs 'microscopic phenomena' over such small scales where the uncertainty principle (among other quantum effects) becomes non-trivial.

However, many real-world phenomena, such as black holes, involve **both** relativistic and quantum effects [9]. Describing such phenomena is very challenging as these two great theories of physics appear incompatible. However, to physicists, it is inconceivable that the universe should be governed by two contradictory sets of laws. Some unified theory should therefore exist, and the search for Quantum Gravity remains an area of active investigation [1, 5].

1.1.1 Search for Quantum Gravity

An exact theory of Quantum Gravity is as yet unknown. This is due to the extreme non-linearity of Einstein's field equations of GR. If these equations were quantized in a manner parallel to the usual quantization of Maxwell's electromagnetic field equations, the resulting quantum theory of gravity is considered 'non-renormalizable' [9]. Renormalization is an essential process of treating divergent parts of quantum theory. Specifically, renormalization absorbs divergences by re-defining some of the original parameters of the theory. Without renormalization, the theory loses predictive power and is generally considered non-fundamental [10]. See Ref. [11] for a full review of this problem.

Many aim to circumvent this renormalization problem by using new approaches such as string theories and loop quantum gravities [9]. Unfortunately, in such theories, the lack of experimental evidence greatly hampers these efforts, and until today, there is no general consensus regarding the quantum effects of gravity.

In order to better understand these effects, advances must be made in experimental observations. To date, there has been limited success in this regard, due to the extreme weakness of gravity relative to the other forces of nature. Additionally, quantum theories of gravity can be extremely complicated,

where even simple calculations are largely intractable. However, an 'effective' quantum theory known as Perturbative Quantum Gravity presents a useful, and much simpler, framework for study of quantum effects of gravity, in the low-energy regime [9, 12].

In the past, this framework has been dismissed as having low experimental value, as the force of gravity is extremely weak in this limit, by necessity. However, as shall be seen in this work, quantum effects of gravity might be observable within these limits and lead to an important application, in Dark Matter research.

1.1.2 Search for Dark Matter

Experiments in modern astronomy have revealed that most of the matter in the universe is dark: all the ordinary matter that can be readily observed comprises just 15 percent of the total matter in the universe, and the rest is called Dark Matter (DM) [13]. The challenge in studying DM arises as it is very difficult to detect, hence the epithet 'dark'. DM is apparently non-luminous, compared to normal matter, although beyond this, little about DM is known with certainty. Many competing models are proposed in the literature, with notable examples: MACHO's (Massive Compact Halo Objects) [14], axions [15], and WIMPS (Weakly Interacting Massive Particles) [16], which are each viable candidates for dark matter. Interestingly, each of these three models suggest that DM is not entirely dark, but there may be weak or indirect interactions with photons or other particles [13, 17].

However, there exist many popular models of DM, which predict that it is entirely dark to everything except gravity. Such models include Klauza-Klein particles [18], quantum/primordial black holes [19], and topological defects [20], among others [13]. Thus, study of DM may be limited solely to the study of its gravitational effects on other matter. Today, this has been exploited through gravitational lensing to reveal a nearly-spherical Dark Matter Halo around our galaxy [21]. However, the exact nature of DM, such as particle mass, is subject to extensive debate. This question will ultimately lead us to an important application of our research on quantum effects of gravity.

1.2 Research Aims

This work considers the effect of gravity on polarized photons. In GR, the gravitational scattering of these photons should be independent of the polarization, due to Einstein's Equivalence Principle, which roughly states that any matter, which is solely under the influence of gravity, will follow

the same null geodesic (i.e., the same path in space-time) regardless of internal composition [6]. Therefore, photon polarization should not affect the scattering of light, classically. However, in a quantum theory of gravity, where gravity is mediated by the exchange of virtual particles (as is true in all other quantum theories), one may calculate non-trivial polarization dependence in the scattering behavior (see Ref. [12] for an example of a similar quantum effect). We chose to focus on scattering linearly polarized photons (versus circularly polarized photons) due to the relative simplicity of representing linear polarization mathematically and since there exist well-known sources of linear polarization, both in nature and produced artificially (see [22] for an interesting example).

The mediator particle of gravity is theorized to be a massless, spin-2 particle, called the graviton [11]. It shall be shown analytically that the coupling between a graviton and a photon *does* depend on the polarization of the photon. Previous research [23, 24, 25] considered this type of graviton-mediated scattering of photons, but did not consider polarization effects.

We find that this polarization dependence is very subtle, due to the weakness of gravity. To detect this quantum effect may require a large number of scattering events. After choosing experimentally realistic parameters, this work introduces a novel Monte-Carlo (MC) simulation to study these quantum effects of gravitational scattering. Our primary application is scattering by Dark Matter. DM, which interacts primarily gravitationally, presents an ideal scattering target, where we can minimize interfering effects of non-gravitational forces. Due to the polarization dependence in gravitational scattering, DM may in fact have polarizing properties even in the simplest scalar models, where DM interacts only through gravity. Ultimately, we chose to model scattering on DM due to the fact that gravity would most likely dominate the interaction (versus the other forces of nature), allowing us to mitigate interfering non-gravitational effects.

1.3 Structure of Thesis

This thesis opens with brief review of the existing literature, contained in Chapter 2. In this chapter, we re-derive several important expressions to support the research. Chapter 3 consists of our novel analytic calculations and derivation of the polarization-dependent scattering machinery of a single photon scattering off a massive scalar particle via graviton exchange. The relevant cross sections and scattering yields for several applications and experimental arrangements is calculated.

These results comprise the bulk of the original work performed in this thesis. We compare our results to prior work done on unpolarized photons, as well.

Chapter 4 then presents our computational results from the Monte-Carlo (MC) simulation. This simulation, written in Python, models a chosen thought experiment involving a strong galactic source of linearly polarized photons which scatter in the Dark Matter Halo surrounding the Milky Way galaxy and are detected on earth. Polarization effects of the light due to this scattering is found to be non-trivial, although the overall effect is small. Chapter 5 includes new calculations for scattering on larger astronomical targets, and Chapters 6 and 7 discuss our analysis, conclusions, and prospects for future research and experiment.

Perhaps the most intriguing future application of our research is the use of simple graviton exchange as an entanglement breaking channel. This effect is briefly explored toward the end of this work, and compared to similar entanglement decoherence due to gravity predicted in the semi-classical framework of Quantum Field Theory in curved spacetime [26, 27]. This may someday present an avenue for future experimentation.

Chapter 2

Theoretical Background

2.1 Perturbative Quantum Gravity

Perturbative Quantum Gravity (PQG) is a formalism which treats the force of gravity as an "Effective" field theory. In the low-energy, weak field limit, PQG is generally considered a good approximation for a quantum theory of gravity (see Ref. [28] for a full review). Essentially, instead of working with the highly non-linear field equations of GR, we approximate gravity as a *linear* theory. Linearized general relativity does not pose the same renormalization issues as traditional GR, and thus PQG provides reasonable predictions of quantum effects of gravity. However, it is important to note that PQG is not a fundamental theory of Quantum Gravity, due to ultraviolet divergences. Rather, PQG is merely an effective theory which appears to work in certain limits. Additional comments on these limits are included in Chapters 5 and 6.

In GR (see [6]), space-time is described using a curved metric $g_{\mu\nu}$. The extent of the curvature at a point on the metric corresponds to the strength of the gravitational field at that location. Whereas GR allows for extremely large integrated curvature (ex. near a singularity), PGQ only allows for small perturbations from the flat space-time metric. More precisely, we assume that that $g_{\mu\nu} = \eta_{\mu\nu} + \kappa h_{\mu\nu}$, where $\eta_{\mu\nu}$ is the flat Minkowski metric, κ is a constant, and $h_{\mu\nu}$ is the perturbation from the flat metric. This linear perturbation represents the effect of gravity as seen by the metric.

As with other quantum field theories, PQG naturally leads to a propagator [29], corresponding to a mediator particle of gravity. Whereas electromagnetism is mediated by photons, the strong force is mediated by gluons, and the weak force is mediated by W and Z bosons, physicists have come to call the mediator of gravity: the Graviton. The rank-2 tensor $h_{\mu\nu}$ can thus be thought as the graviton field

(see Appendix A for discussion of tensors). Our first task is to derive the graviton propagator to be used in our study of particle interactions via graviton exchange.

2.2 Deriving the Graviton Propogator

The following section involves several topics from GR and PQG, for which brief comments and explanations are offered. For a more detailed review, see Ref. [29, 30, 28], although we will refer to most of these topics only in passing.

We begin with the Einstein-Hilbert action (S) for gravity, which is given by

$$S = \frac{1}{16\pi G} \int d^4x \sqrt{-g} R, \quad (2.1)$$

where $g = \det(g_{\mu\nu})$, G is Newton's constant, and R is the scalar curvature, to be defined momentarily. It is a standard GR exercise to 'vary the action' meaning, to consider what happens to S if we perturb the metric by a tiny amount. After performing these manipulations, we can actually find the famous Einstein field equations

$$R_{\mu\nu} - \frac{1}{2}g_{\mu\nu}R = -8\pi GT_{\mu\nu}, \quad (2.2)$$

where $T^{\mu\nu}$ is the stress-energy tensor, which encodes the matter fields of the universe and $R_{\mu\nu}$ is the Ricci Tensor [29] To define the Ricci tensor $R_{\mu\nu}$ and the scalar curvature R , recall the Riemann curvature tensor

$$R_{\mu\nu\kappa}^{\lambda} = \partial_{\nu}\Gamma_{\mu\kappa}^{\lambda} - \partial_{\kappa}\Gamma_{\mu\nu}^{\lambda} + \Gamma_{\mu\kappa}^{\sigma}\Gamma_{\nu\sigma}^{\lambda} - \Gamma_{\mu\nu}^{\sigma}\Gamma_{\kappa\sigma}^{\lambda}, \quad (2.3)$$

where we use the usual Riemann-Christoffel symbols

$$\Gamma_{\mu\nu}^{\lambda} = \frac{1}{2}g^{\lambda\rho}(\partial_{\nu}g_{\rho\mu} + \partial_{\mu}g_{\rho\nu} + \partial_{\rho}g_{\mu\nu}). \quad (2.4)$$

Now, the Ricci Tensor is defined by simply contracting the indices $R_{\mu\kappa} \equiv R_{\mu\nu\kappa}^{\nu}$. The scalar curvature is then defined as $R \equiv g^{\mu\nu}R_{\mu\nu}$.

Overall, this gravitational action may seem very different from those of the other field theories [29]. Typically, space-time is merely a fixed background for the interactions, whereas here, the metric

is a dynamical quantity, which itself governs the strength of the gravitational field. Nonetheless, this action can be massaged into a more familiar structure, permitting easier study of gravitational field theory [29].

Let us explicitly assume the weak field approximation of PQG where $g_{\mu\nu} = \eta_{\mu\nu} + \kappa h_{\mu\nu}$. With this assumption, we may expand the action in terms of $h_{\mu\nu}$. This linearizes the effect of gravity. A short glance at the equations above indicates that the scalar curvature R involves two partial derivatives of $g_{\mu\nu}$ in its definition. This means that the weak field expansion of S includes the factor

$$\partial h \partial h + h \partial h \partial h + h^2 \partial h \partial h + \dots \quad (2.5)$$

Here, the first term describes the graviton propagator and the later terms describe how the graviton interacts with itself, which we will drop due to their incredible weakness. Notice that we temporarily dropped the indices for convenience.

We must now remember to include the graviton coupling to matter in our action. This can be done using the stress-energy tensor $T^{\mu\nu}$ in flat spacetime, which describes all the matter fields in the universe. We thus need only to add the following term to the action, S

$$S' = S - \int d^4x \frac{1}{2} h_{\mu\nu} T^{\mu\nu}. \quad (2.6)$$

Expanding the complete action to second order $O(h^2)$, keeping careful track of the indices, we get the form

$$S' = \int d^4x \left(\frac{1}{32\pi G} I - \frac{1}{2} h_{\mu\nu} T^{\mu\nu} \right), \quad (2.7)$$

where I is the invariant quantity

$$I \equiv \frac{1}{2} \partial_\lambda h^{\mu\nu} \partial^\lambda h_{\mu\nu} - \frac{1}{2} \partial_\lambda h_\mu^\mu \partial^\lambda h_\nu^\nu - \partial_\lambda h^{\lambda\nu} \partial^\mu h_{\mu\nu} + \partial^\nu h_\lambda^\lambda \partial^\mu h_{\mu\nu}. \quad (2.8)$$

See Ref. [29] for additional details of this derivation. If we then impose the harmonic gauge condition (which we will discuss later)

$$\partial_\mu h_\nu^\mu = \frac{1}{2} \partial_\nu h_\lambda^\lambda, \quad (2.9)$$

we kill the second and last terms of I . We note that a gauge condition is merely a technique to relate redundant degrees of freedom. As an analogy, consider that any rotation of a perfect sphere would leave the sphere invariant. In this simple analogy, a gauge condition would essentially negate the effect of rotation. In a similar way, the harmonic gauge removes unnecessary degrees of freedom in GR. Specifically, GR explains that physics occurs independent of any coordinate system that we choose, and the harmonic gauge is a way of relating all coordinate systems [6]. A similar gauge condition will be employed later.

In this harmonic gauge, the action becomes

$$\begin{aligned} S' &= \int d^4x \frac{1}{2} \left(\frac{1}{32\pi G} \left(\partial_\lambda h^{\mu\nu} \partial^\lambda h_{\mu\nu} - \frac{1}{2} \partial_\lambda h_\mu^\mu \partial^\lambda h_\nu^\nu \right) - h_{\mu\nu} T^{\mu\nu} \right) \\ &= \frac{1}{32\pi G} \int d^4x \left(h^{\mu\nu} K_{\mu\nu;\lambda\sigma} (-\partial^2) h^{\lambda\sigma} - h_{\mu\nu} T^{\mu\nu} \right). \end{aligned} \quad (2.10)$$

Here $K_{\mu\nu;\lambda\sigma} \equiv \frac{1}{2}(\eta_{\mu\lambda}\eta_{\nu\sigma} + \eta_{\mu\sigma}\eta_{\nu\lambda} - \eta_{\mu\nu}\eta_{\lambda\sigma})$ is the matrix we must invert to build the graviton propagator [29], in analogy with the electromagnetic propagator. We note, as above, that the graviton field $h_{\mu\nu}$ is coupled to the entire stress-energy tensor $T^{\mu\nu}$. As the stress energy tensor encodes all the energy/matter in the universe, this reflects that *everything* is subject to the graviton field and the effect of gravity, as expected from GR. From the convenient fact that $K = K^{-1}$, we find the propagator

$$D_{\mu\nu;\lambda\sigma}(k) = \frac{1}{2} \frac{\eta_{\mu\lambda}\eta_{\nu\sigma} + \eta_{\mu\sigma}\eta_{\nu\lambda} - \eta_{\mu\nu}\eta_{\lambda\sigma}}{k^2 + i\epsilon}, \quad (2.11)$$

where k is the momentum transferred by the graviton exchange and ϵ is some infinitesimal quantity. We shall use this graviton propagator $D_{\mu\nu;\lambda\sigma}(k)$ in our study of graviton exchange.

Our research focuses on a particular type of interaction, namely, the scattering of a photon on a scalar target. We have chosen a scalar target since a scalar particle is defined to have spin-0 and positive parity. It is convenient that scalar particles do not show any interfering spin effects. In order to study such an interaction from a quantum field-theoretic perspective, we must certainly calculate the photon-photon-graviton vertex as used in Ref. [23, 24], which couples a photon with the graviton, and in the next section we calculate this vertex from the relevant Lagrangian.

2.3 Scattering Fundamentals

We begin with the Lagrangian for the electromagnetic field coupled to the graviton field (see [30] for an introduction):

$$\mathcal{L} = \sqrt{-g} \left(-\frac{1}{4} g^{\mu\nu} g^{\alpha\beta} F_{\mu\alpha} F_{\nu\beta} \right), \quad (2.12)$$

where $\sqrt{-g} = \sqrt{-\det(g_{\mu\nu})}$ as before. Here, $F_{\mu\nu}$ is the EM tensor, defined as the exterior derivative of the EM four-potential vector A^μ

$$F^{\mu\nu} = \partial^\mu A^\nu - \partial^\nu A^\mu. \quad (2.13)$$

In our weak-field approximation $g_{\mu\nu} = \eta_{\mu\nu} + \kappa h_{\mu\nu}$, we expand the gravitational metric to first order¹ in κ . More details about the notation and conventions can be found in Appendix A.

$$\begin{aligned} g^{\mu\nu} g^{\alpha\beta} F_{\mu\alpha} F_{\nu\beta} &\approx (\eta^{\mu\nu} \eta^{\alpha\beta} - \kappa h^{\mu\nu} \eta^{\alpha\beta} - \kappa h^{\alpha\beta} \eta^{\mu\nu}) F_{\mu\alpha} F_{\nu\beta} \\ &= \eta^{\mu\nu} \eta^{\alpha\beta} F_{\alpha\mu} F_{\beta\nu} + \kappa h_\nu^\mu \eta^{\nu\nu} \eta^{\alpha\beta} F_{\mu\alpha} F_{\beta\nu} + \kappa h_\beta^\alpha \eta^{\beta\beta} \eta^{\mu\nu} F_{\mu\alpha} F_{\beta\nu} \\ &= F^{\mu\nu} F_{\mu\nu} + 2\kappa h_\nu^\mu F_{\mu\alpha} F^{\alpha\nu}. \end{aligned} \quad (2.14)$$

Our simplification uses the antisymmetry of the EM-tensor $F_{\mu\nu} = -F_{\nu\mu}$, and we raise and lower the indices of $F_{\mu\nu}$ and $h^{\mu\nu}$ as needed. Using the additional approximation common to the literature, $\sqrt{-g} \approx 1 + \frac{\kappa}{2} \eta_{\alpha\beta} h^{\alpha\beta}$, we find the full Lagrangian becomes

$$\mathcal{L} = \left(1 + \frac{\kappa}{2} \eta_{\alpha\beta} h^{\alpha\beta} \right) \left[-\frac{1}{4} (F^{\mu\nu} F_{\mu\nu} + 2\kappa h_\nu^\mu F_{\mu\rho} F^{\rho\nu}) \right]. \quad (2.15)$$

We distribute and collect the terms for the interaction Lagrangian, keeping only those terms to the first order² in κ

$$\mathcal{L}_{int} = -\frac{\kappa}{8} \eta_{\alpha\beta} h^{\alpha\beta} F^{\mu\nu} F_{\mu\nu} + \frac{\kappa}{2} h_\nu^\mu F_{\mu\rho} F^{\rho\nu}. \quad (2.16)$$

So, after simplification, we obtain six terms of our Interaction Lagrangian

¹We expand to first order since the κ -terms govern the EM-gravity coupling, whereas all κ^2 -terms denotes the graviton field coupling with itself.

²i.e., we drop the constant terms, which govern the EM coupling with itself

$$\begin{aligned}
\mathcal{L}_{int} = & -\frac{\kappa}{4}\eta_{\alpha\beta}h^{\alpha\beta}\partial_{\mu}A_{\nu}\partial^{\mu}A^{\nu} + \frac{\kappa}{4}\eta_{\alpha\beta}h^{\alpha\beta}\partial_{\mu}A_{\nu}\partial^{\nu}A^{\mu} - \frac{\kappa}{2}h^{\mu\nu}\partial_{\mu}A_{\rho}\partial^{\rho}A_{\nu} \\
& + \frac{\kappa}{2}h^{\mu\nu}\partial_{\rho}A_{\mu}\partial^{\rho}A_{\nu} + \frac{\kappa}{2}h^{\mu\nu}\partial_{\mu}A_{\rho}\partial_{\nu}A^{\rho} - \frac{\kappa}{2}h^{\mu\nu}\partial_{\rho}A_{\mu}\partial_{\nu}A^{\rho}.
\end{aligned} \tag{2.17}$$

Now, it is only a matter of applying Feymann Rules to calculate each photon-photon-graviton vertex. We use the Feynman Rules derived for a spin two particle [31] in the massless limit [32] (see Ref. [9, 10] for a modern review). The calculations yield 10 terms as follows

$$\begin{aligned}
V_{k_1,k_2} = & \frac{i\kappa}{2}[k_1 \cdot k_2(\eta^{\rho\alpha}\eta^{\beta\sigma} - \eta^{\rho\beta}\eta^{\alpha\sigma} - \eta^{\rho\sigma}\eta^{\alpha\beta}) + \eta^{\rho\sigma}k_1^{\beta}k_2^{\alpha} + \eta^{\alpha\beta}k_1^{\rho}k_2^{\sigma} - \eta^{\alpha\beta}k_1^{\sigma}k_2^{\rho} \\
& - (\eta^{\alpha\rho}k_2^{\sigma}k_1^{\beta} + \eta^{\beta\rho}k_2^{\rho}k_1^{\beta} + \eta^{\beta\rho}k_1^{\sigma}k_2^{\alpha} - \eta^{\beta\sigma}k_1^{\rho}k_2^{\alpha})],
\end{aligned} \tag{2.18}$$

where k denotes the relativistic momentum and the subscripts 1 and 2 refer to the incoming and outgoing particles, respectively. This is the vertex that we shall use in our study of the photon-scalar interaction via graviton exchange, (which is confirmed by Ref. [33]).

Chapter 3

Scattering Machinery

3.1 Photon-Scalar Scattering

We begin our study of the quantum gravitational scattering of light by first considering a much simpler example from quantum electrodynamics (QED). Consider the two Feynman diagrams below (Fig 3.1). On the left is the diagram representing the desired photon-scalar scattering via graviton exchange, while on the right is the lowest order diagram for electron-muon scattering via photon exchange. The scattering machinery for either case are extracted from the relevant Feynman Rules. We recall that a Feynman diagram is merely a convenient visualization of a perturbative contribution to a quantum amplitude. Such an amplitude governs the transition from an initial state of a system to a final state. We must use the Feynman rules to translate from the first order diagrams below to scattering amplitudes which will be used to define the probability of the chosen scattering.

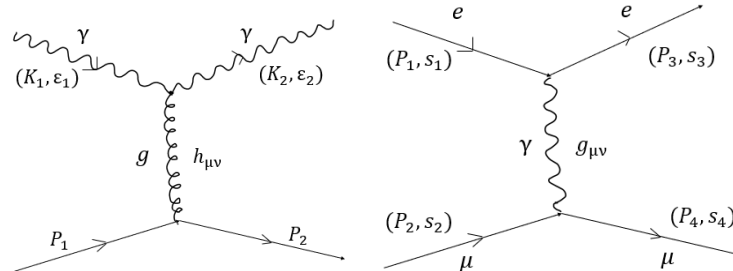


Fig. 3.1 Photon-Scalar Scattering via graviton exchange (left) and Electron-Muon Scattering via photon exchange (right).

The Feynman rules for the analogous QED case (depicted by Fig. 3.1 on the right) are fairly simple: we associate incoming fermions with a spinor $u(s, p)$ and outgoing fermions with the spinor

$\bar{u}(s, p)$ for particles of momentum p and spin s . Here, spinors are the complex vector solutions to the Dirac Equation, which is the wave equation that describes spin- $\frac{1}{2}$ fermions like electrons and muons [29]. We attach the factor $ie\gamma^\mu$ to each vertex, and since our particles exchange a virtual photon, we introduce the EM propagator $-ig_{\mu\nu}/(q^2 + i\epsilon)$ (see Ref. [29]). This leads to the scattering amplitude represented by the following:

$$i\mathcal{M} = (ie)\bar{u}(s_3, P_3)\gamma^\mu u(s_1, P_1)\frac{-ig_{\mu\nu}}{q^2 + i\epsilon}(ie)\bar{u}(s_4, P_4)\gamma^\nu u(s_2, P_2). \quad (3.1)$$

Here, γ^μ denote a special set of 4x4 matrices,¹ important in QED

$$\gamma^0 = \begin{pmatrix} I & 0 \\ 0 & -I \end{pmatrix}, \quad \gamma^i = \begin{pmatrix} 0 & \sigma^i \\ -\sigma^i & 0 \end{pmatrix}, \quad (3.2)$$

where I is the 2×2 identity matrix and σ^i are the familiar Pauli matrices of quantum mechanics. We also note the relationship between spinors $\bar{u} \equiv u^\dagger \gamma^0$. See Appendix B for additional details about electron-muon scattering.

In a completely analogous way, we build the scattering amplitude for photon-scalar scattering via graviton exchange. The associated scattering amplitude with this two body scattering is

$$i\mathcal{M} = i[u(K_1, \epsilon_1)V_{K_1, K_2}\bar{u}(K_2, \epsilon_2)]D_{\mu\nu, \lambda\sigma}[v(P_1)V_{P_1, P_2}\bar{v}(P_2)], \quad (3.3)$$

where the K, P denote the momenta of the photon and scalar particles, ϵ denotes photon polarization, and the subscripts 1 and 2 denote initial and final quantities, respectively. Note that the scalar particle with momentum P carries no polarization. The spinors u, \bar{u}, v, \bar{v} represent the relevant arms of the Feynman diagram, V represents the relevant vertex (see Eq. 2.19), and $D_{\mu\nu, \lambda\sigma}$ is the graviton propagator (Eq. 2.11).

In order to proceed further, we must set up the scattering kinematics and define the polarization vectors of the photons. This will eventually lead us to the cross sections and additional scattering machinery.

¹These matrices are said to form a ‘Clifford Algebra’ due to anti-commutation relation $\{\gamma^\mu, \gamma^\nu\} = 2\eta^{\mu\nu}$

3.1.1 Scattering Kinematics

We now set up the kinematics for photon-scalar scattering via graviton exchange. Let K_1, K_2 denote the 4-momentum of the initial and final photon respectively, and P_1, P_2 denote that of the initial and final scalar particles. In the center-of-momentum (CoM) frame (where $\vec{K}_1 = -\vec{P}_1$) we have

$$\begin{aligned} K_1 &= (K, 0, 0, K), \\ K_2 &= (K, K\sin\theta, 0, K\cos\theta), \\ P_1 &= (P, 0, 0, -K), \\ P_2 &= (P, -K\sin\theta, 0, -K\cos\theta), \end{aligned}$$

Observe that this 2-body scattering is elastic and is in the relativistic limit, where $K_1^0 = K_2^0$ and $P_1^0 = P_2^0$. We also define the usual scalar product of 4-momentum $P = (E, \vec{P})$ and $P' = (E', \vec{P}')$ as

$$PP' = EE' - P_x P'_x - P_y P'_y - P_z P'_z = M_p^2. \quad (3.4)$$

In other words, we implicitly contract 4-momenta with the Minkowski metric, using the sign convention $(+, -, -, -)$.

3.1.2 Photon Polarization

Our research involves gravitational scattering of polarized photons. We therefore make several comments about photon polarization. In the literature, there are many conventions, so we outline basic ideas and background here.

In quantum mechanics, spin is a measure of the intrinsic angular momentum of an elementary particle. Spin is quantized, meaning that there are only particular spin values which may be observed. Which values are allowed is determined by the type of particle. Of interest to us are bosons, which carry integer spin $0, 1, 2, \dots$. For example, the photon is spin 1 and the graviton is spin 2. Other particles, known as fermions, carry half-integer spin, such as the electron which is spin- $\frac{1}{2}$. For a particle with spin- S , there are $2S + 1$ possible values of spin which can be observed; these values are evenly spaced integers or half integers between $+S$ and $-S$, see textbook such as [7].

Hence, there are three distinct eigenstates of a spin-1 particle: $+1$, 0 , and -1 . However, as the photon is a massless spin-1 particle, it may only carry spin $+1$ and -1 . We shall refer to these spin states as spin up and spin down ¹ or $|U\rangle$ and $|D\rangle$. Thinking in terms of the ‘right hand rule’ of Calculus, spin up corresponds to a counter-clockwise rotation of the oscillating electric and magnetic fields that comprise the photon, whereas spin down determines a clockwise rotation. These two rotations are always transverse to the direction of motion, and correspond to the classical left and right circular polarization of light.

However, to simplify our calculations, we avoid circular and elliptical polarization, and instead focus on *linear* polarization which are easier to represent mathematically. Additionally, linearly polarized photons are readily accessible for future experimental applications, as they are abundant in nature and can be produced in a lab (see Ref. [22] for an interesting example). Specifically, linearly polarized photons are defined in terms of particular superpositions of the aforementioned up and down states. The two orthogonal eigenstates of linear polarization are commonly denoted as horizontal and vertical polarization states $|H\rangle$ and $|V\rangle$

$$\begin{aligned} |H\rangle &= \frac{-i}{\sqrt{2}}(|U\rangle - |D\rangle) \\ |V\rangle &= \frac{1}{\sqrt{2}}(|U\rangle + |D\rangle). \end{aligned} \tag{3.5}$$

These correspond, to classical linearly polarized light. With this choice, we can happily denote photon polarization using a simple vector oriented in some direction transverse to the direction of motion.

We now choose basis vectors for the photon polarization. As is typical [24], we choose one vector, e^{\parallel} within the plane spanned by K_1, K_2 , and the other vector, e^{\perp} , we choose as orthogonal to this scattering plane. Following the conventions in Ref. [23], we write

$$\begin{aligned} e_1^{\perp} &= (0, 1, 0) \\ e_2^{\perp} &= (0, 1, 0) \\ e_1^{\parallel} &= (1, 0, 0) \\ e_2^{\parallel} &= (-\cos\theta, 0, \sin\theta), \end{aligned} \tag{3.6}$$

¹Certainly the spin state of a photon may be in a superposition of the up and down states

Here the subscripts 1 and 2 denote initial and final polarization. As expected (due to conservation laws), the components of e^\perp are invariant under scattering, while e^\parallel rotates in the scattering plane [24] (see Fig. 3.2-3 below¹). We assume the gauge condition $e^0 = 0$.

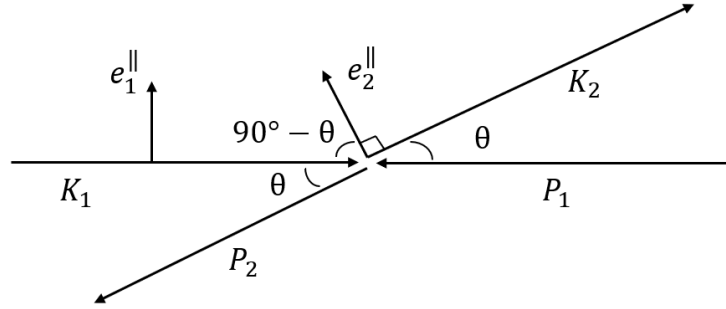


Fig. 3.2 Rotation of polarization basis vector in the scattering plane.

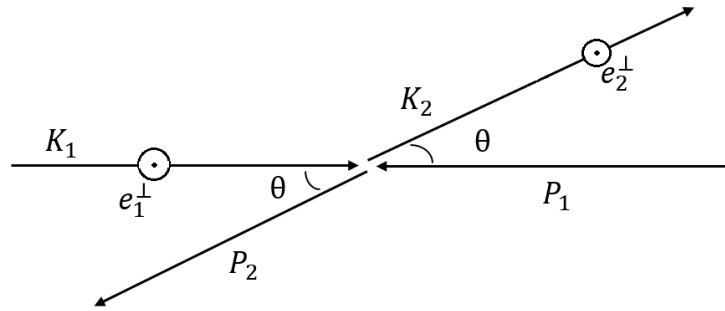


Fig. 3.3 Rotation of polarization basis vector which is orthogonal to the scattering plane.

3.2 Polarization Effects

Following Ref. [23], we calculate the matrix elements for arbitrary initial and final polarization using Feynman rules and the appropriate interaction Lagrangian of effective quantum gravity. We find the matrix element

¹It is important to recall that the two depicted states are quantum states, i.e., there is no continuous change of polarization between e^\parallel and e^\perp . Just as there are only two possible circular states, so to, these are the *only* possible states of linear polarization

$$\begin{aligned} \langle K_2, P_2 | M | K_1, P_1 \rangle = & \frac{\lambda^2 \delta^4(K_2 + P_2 - K_1 - P_1)}{4(2\pi)^2 \sqrt{K_1^0 K_2^0 P_1^0 P_2^0}} \frac{4}{-2K_1 K_2} \\ & \{ (e_{(\rho}^2 K_{\alpha}^2 - e_{\alpha}^2 K_{\rho}^2)(e_{\sigma}^1 K_1^{\alpha} - e_1^{\alpha} K_{\sigma}^1) - \frac{1}{4} \delta_{\rho\sigma} (e_{\alpha}^2 K_{\beta}^2 - e_{\beta}^2 K_{\alpha}^2)(e_1^{\alpha} K_1^{\beta} - e_1^{\beta} K_1^{\alpha}) \} \\ & \cdot \left[p_1^{(\rho} p_2^{\sigma)} - \frac{1}{2} m^2 \delta^{\rho\sigma} \right], \quad (3.7) \end{aligned}$$

where Greek indices represent components of 4-vectors and the numbers 1, 2 correspond to initial and final particles respectively.

The quantity $\lambda = \sqrt{8\pi G}$ governs the strength of the gravitational interaction and $\delta^{\rho\sigma}$ is the usual Kronecker delta and $A_{(\rho} B_{\sigma)}$ denotes symmetrization with respect to the indices ρ and σ , as defined in Appendix A.

For scalar particles, we know $P_1^{\rho} P_2^{\sigma} = P_1^{\sigma} P_2^{\rho}$ due to boson symmetry. Hence, we simplify $p_1^{(\rho} p_2^{\sigma)} = P_1^{\rho} P_2^{\sigma}$. The symmetrization of the expression in the curly brackets (in Eq. (4) above) is less trivial

$$\begin{aligned} (e_{(\rho}^2 K_{\alpha}^2 - e_{\alpha}^2 K_{\rho}^2)(e_{\sigma}^1 K_1^{\alpha} - e_1^{\alpha} K_{\sigma}^1) = \\ \frac{1}{2} \left[(e_{\rho}^2 K_{\alpha}^2 - e_{\alpha}^2 K_{\rho}^2)(e_{\sigma}^1 K_1^{\alpha} - e_1^{\alpha} K_{\sigma}^1) + (e_{\sigma}^2 K_{\alpha}^2 - e_{\alpha}^2 K_{\sigma}^2)(e_{\rho}^1 K_1^{\alpha} - e_1^{\alpha} K_{\rho}^1) \right]. \end{aligned} \quad (3.8)$$

Substituting this expression back into Eq. (4), we distribute and simplify by contracting the 4-vectors having equivalent indices.

This contraction produces several occurrences of the scalar products $P_1 e_1, P_2 e_2, K_1 e_1$ and $K_2 e_2$, which are equal to zero in the CoM, since the polarization of light is transverse to the direction of motion. Including only the nonzero terms, and grouping like terms, we obtain the full expression

$$\begin{aligned}
\langle K_2, P_2 | M | K_1, P_1 \rangle &= \frac{\lambda^2 \delta^4(K_2 + P_2 - K_1 - P_1)}{4(2\pi)^2 \sqrt{K_1^0 K_2^0 P_1^0 P_2^0}} \frac{4}{-2K_1 K_2} \\
&\frac{1}{2} ((P_1 e_2)(P_2 e_1)(K_1 K_1) - (P_1 e_2)(P_2 K_1)(K_2 e_1) - (P_1 K_2)(P_2 e_1)(K_1 e_2) + (P_1 K_2)(P_2 K_1)(e_1 e_2)) \\
&\quad - \frac{1}{4} (-2(P_1 P_2)(K_1 K_2)(e_1 e_2) + 2(P_1 P_2)(K_1 e_2)(K_2 e_1)) \\
&\quad - \frac{1}{2} m^2 (2(K_1 e_2)(K_2 e_1) - 2(e_1 e_2)(K_1 K_2)) + \frac{1}{8} m^2 \delta^{\rho\sigma} \delta_{\rho\sigma} (2(K_1 e_2)(K_2 e_1) - 2(e_1 e_2)(K_1 K_2)). \quad (3.9)
\end{aligned}$$

Now, due to properties of the Kronecker delta, $\delta^{\rho\sigma} \delta_{\rho\sigma} = \delta^{\rho\rho} \delta_{\sigma\sigma} = \delta^{\rho\rho} = 4$. We may thus cancel the final two terms, leaving exactly 6 terms

$$\begin{aligned}
\langle K_2, P_2 | M | K_1, P_1 \rangle &= \frac{-\lambda^2 \delta^4(K_2 + P_2 - K_1 - P_1)}{4(2\pi)^2 K P} \frac{1}{K_1 K_2} \\
&\cdot \{ (K_1 K_2)(e_2 P_1)(e_1, P_2) - (e_2 K_1)(K_2 P_1)(e_1 P_2) - (e_1 k_2)(e_2 P_1)(K_1 P_2) \\
&\quad + (e_1 e_2)(K_2 P_1)(K_1 P_2) - (e_1 e_2)(K_1 K_2)(P_1 P_2) + (e_1 K_2)(e_2 K_1)(P_1 P_2) \}. \quad (3.10)
\end{aligned}$$

For convenience, we now use $K = K_i^0$ and $P = P_i^0$ for $i = 1, 2$, thus associating K with the photon energy and P with the energy of the scalar particle. We also correct an error in Ref. [23], where a seventh term was mistakenly included.

By plugging our kinematics into the corrected equation above, we obtain for the sum in curly brackets (for some specified initial and final polarization states)

$$\begin{aligned}
e_1^{\parallel} \rightarrow e_2^{\parallel} &: K^2 (K + P)^2 \cos\theta \\
e_1^{\parallel} \rightarrow e_2^{\perp} &: 0 \\
e_1^{\perp} \rightarrow e_2^{\parallel} &: 0 \\
e_1^{\perp} \rightarrow e_2^{\perp} &: K^2 (K + P)^2.
\end{aligned} \quad (3.11)$$

Thus our non-zero, polarization-dependent matrix elements, which governs the probability of the transition between initial and final states of our system, become

$$\begin{aligned}\langle K_2, P_2 | M_{\parallel\parallel} | K_1, P_1 \rangle &= \frac{-\lambda^2 \delta^4(K_2 + P_2 - K_1 - P_1)(K + P)^2}{4(2\pi)^2 P} \frac{\cos\theta}{1 - \cos\theta}, \\ \langle K_2, P_2 | M_{\perp\perp} | K_1, P_1 \rangle &= \frac{-\lambda^2 \delta^4(K_2 + P_2 - K_1 - P_1)(K + P)^2}{4(2\pi)^2 P} \frac{1}{1 - \cos\theta}.\end{aligned}\quad (3.12)$$

3.2.1 Differential Cross Section

In scattering theories, there are well-known expressions which relates the invariant amplitude M above to the differential cross section (in the CoM frame). In general,

$$\frac{d\sigma}{d\Omega_{CoM}} \propto |M|^2,$$

where M represents matrix elements derived via Feynman rules, as done above. Following the lead of Ref. [23, 24] our matrix elements, Eq. 3.12, above leads us to the polarization-dependent cross sections

$$\begin{aligned}\frac{d\sigma_{\parallel\parallel}}{d\Omega} &= \frac{\lambda^4 (K + P)^4 \cos^2\theta}{16(2\pi)^2 P^2 (1 - \cos\theta)^2}, \\ \frac{d\sigma_{\perp\perp}}{d\Omega} &= \frac{\lambda^4 (K + P)^4}{16(2\pi)^2 P^2 (1 - \cos\theta)^2}.\end{aligned}\quad (3.13)$$

We will discuss the dependencies of this cross section at the end of this chapter. However, we immediately recognize a fascinating point of interest concerning these cross sections. Specifically, the largest difference in cross section is at angles near 90 degrees. In fact, we observe that for one polarization, there is no 90 degree scattering, while the other polarization has non-trivial likelihood of 90 degree scattering.

3.2.2 Unpolarized Photons

Our results also lead to the unpolarized cross sections, by summing over all initial and averaging over final polarization states presented in Eq. (3.13)

$$|M|^2 = \sum_{pol.} |M_{if}|^2. \quad (3.14)$$

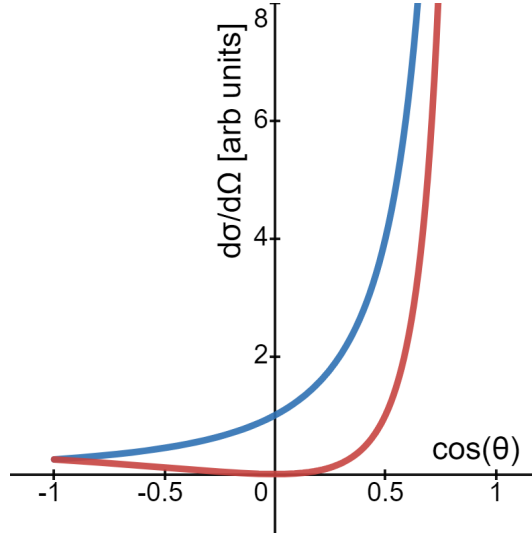


Fig. 3.4 Shape of differential cross section as a function of scattering angle θ (averaged over all azimuthal angles ϕ). Blue and Red curves correspond to initial polarization e^\perp and e^\parallel respectively for a 511 KeV photon scattering off a scalar particle.

This leads to the differential cross section

$$\frac{d\sigma}{d\Omega} = \frac{\lambda^4(K+P)^4}{16(2\pi)^2P^2} \frac{1 + \cos^2\theta}{(1 - \cos\theta)^2}. \quad (3.15)$$

However, in Ref. [23], the differential cross section for unpolarized photons is given as

$$\frac{d\sigma}{d\Omega} = \frac{\lambda^4(K+P)^4}{16(2\pi)^2P^2} \frac{(1 + \cos\theta)^2}{(1 - \cos\theta)^2}, \quad (3.16)$$

which includes ‘interference terms’. Similarly in Ref. [24]. There, the authors seem to consider a photon whose initial polarization is given by a mixed state, i.e., is in a superposition of possible basis states, leading to the above interference terms. In contrast, our result should apply to a collection of photons in a pure state, where there is an equal distribution of photons with either polarization (but each photon individually has some definite state), leading to no interference terms. The figure below compares the shape of both options, which display the same long-term behavior.

3.2.3 Total Cross Sections

To calculate the polarization-dependent total cross section σ , we integrate using spherical coordinates

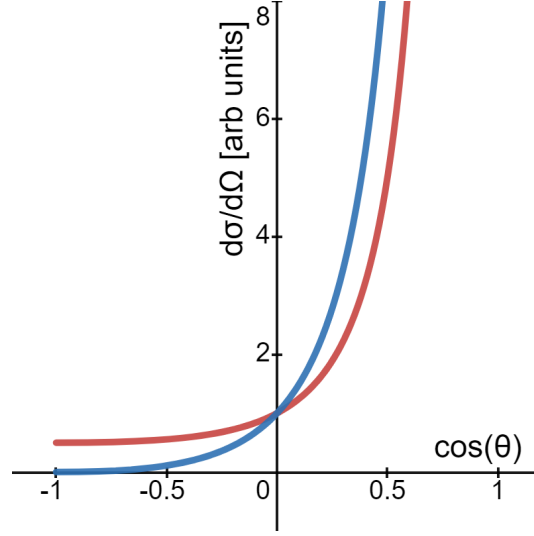


Fig. 3.5 Shape of unpolarized cross section, where red and blue curves correspond to our results for unpolarized photons given in Eq. 3.15 and the analogous results of Ref. [23] in Eq. 3.16, respectively.

$$\sigma = \int \frac{d\sigma}{d\Omega} d\Omega = \int_0^{2\pi} d\phi \int_0^\pi \frac{d\sigma}{d\Omega} \sin\theta d\theta. \quad (3.17)$$

Integrating over all solid angles, we find that

$$\sigma_{\parallel\parallel} = \frac{\lambda^4(K+P)^4}{16(2\pi)^2 P^2} \int_0^{2\pi} d\phi \int_0^\pi \frac{\sin\theta}{(1-\cos\theta)^2} d\theta = \infty, \quad (3.18)$$

$$\sigma_{\perp\perp} = \frac{\lambda^4(K+P)^4}{16(2\pi)^2 P^2} \int_0^{2\pi} d\phi \int_0^\pi \frac{\cos^2\theta \sin\theta}{(1-\cos\theta)^2} d\theta = \infty, \quad (3.19)$$

reflecting the infinite range of gravity. However, the shape of the integral implies that at distances near $\pm\infty$ from the target scalar particle, the strength of the interaction is very weak and likelihood of scattering is essentially zero, meaning that the average scattering angle will be at or very near 0, as expected intuitively.

3.2.4 Likelihood of Scattering

Due to the presence of λ^4 , we notice that the coefficient of the differential cross section is proportional to G^2 and (assuming that the energy of the scalar particle is much larger than the photon energy $P \gg K$) it is also proportional to P^2 . In our weak field approximation, we should consider only small P , and thus, we expect very small cross sections in reasonable scattering scenarios. However,

there is still non-zero probability that an ‘interesting’ or large angle scattering event will occur. We are interested in large angles since the largest polarization dependence occurs in such scattering.

Unfortunately, when scattering a single photon, we expect only trivial or small angle scattering (as the cross section is largest near 0 degrees). This cross section serves statistically as a type of probability density function with low likelihood of large angle scattering. However, with a strong enough source of photons, we may yet be able to detect polarization dependence of gravity scattering.

This motivates some new definitions. Specifically, we define the number of scattering events, also known as the yield, as $J = L\sigma$ where $L = \Phi\rho_t l$ is the Luminosity. Here, Φ represents the photon flux of photons through the target, ρ_t is the number density of the target, and l is the length of the target. We shall discuss reasonable parameters for Φ and l for a variety of applications in the next chapters. Also, we observe that the number density of the target $\rho_t = N/V$ where N is the number of target particles and V is the volume of the target.¹

We consider the dependence of the scattering yield on mass of the scalar target. Consider scattering on a cloud of matter with fixed mass M . Supposing this cloud is composed of N massive scalar particles, each with mass m , we observe that the number density ρ_t is inversely proportional to the individual mass m . From our results above, we observe that $\sigma \propto m^2$ and $L \propto \rho_t \propto m^{-1}$. We thus determine that $J \propto m$. Hence, the number of scattering events is sensitive to mass of the target scalar particle. Thus, a target consisting of many heavy particles should produce more scattering than another target consisting of many light particles - even if the total mass in both cases is equivalent! This result, that the scattering yield is directly proportional to the particle mass, will be very important in the next two sections, where we develop applications of our research.

¹Note: this quantity is also related to mass density, as $\rho_t = (N_A/M)\rho_m$ where M is the molar mass of the target particles, N_A is Avagadro’s number, and ρ_m is the usual mass density

Chapter 4

Gravitational Polarization by Dark Matter

We have seen that gravitational effects are generally very subtle compared to those of electromagnetism. To illustrate, recall that EM electron-muon scattering has an effect which is many orders of magnitude larger than that of the analogous gravitational scattering of light. To study the desired quantum gravitational phenomenon, we need physical parameters which lead to nontrivial probability of light polarization by graviton exchange, without interfering EM or weak effects. We thus focus on a particular type of matter, for which interactions are likely to be dominated by gravity: Dark Matter (DM). This provides an ideal experimental scenario, where we need be less concerned about interfering electromagnetic or weak effects.

As mentioned in the introduction, DM models predict a diverse range of possible interactions with ordinary luminous matter [17]. In most cases, DM does not couple directly with photons - hence the term dark [13]. Further, there is a large class of models, which predict that DM can *only* interact gravitationally. In any case, it is inevitable that light should scatter gravitationally on DM particles. Our analytical results from Chapter 3 indicate that even given the most typical, scalar models of DM, this scattering will induce polarization, which essentially gives DM properties of a polarimeter.

Also, our results indicate that the probability of light scattering (and polarization) is dependent on the mass of the target particle. This permits the possibility of introducing new upper-limits for the mass of DM particles, as will be discussed in more detail below. Given the tremendous range of masses predicted by different models of DM, this is a very intriguing application.

4.1 Galactic Halo

Let us consider a strong source of photons at the center of our Milky Way galaxy, emitted isotropically. These photons are ejected into the roughly-spherical galactic halo of (DM) particles. The vast majority of these photons would likely continue on a straight, undisturbed trajectory, but a few photons may scatter at large angles, and these scattered photons may be detected by a device on Earth. Given our results, gravity-induced polarization¹ may subsequently be observed!

As the luminosity is proportional to the target number density, it is vital to choose an appropriate density profile for the Dark Matter Halo. There are two general types of models for the density profile [21]. The first type are known as Cored Halo models which display a central ‘plateau’ of finite density, and beyond some scale radius, the density decreases proportional to the cube of the radius. The second type are known as Central Cusp models, which predict an infinitely increasing central peak (with similar long-term growth $\rho \propto r^{-3}$). See Fig 4.1 below which compares the two types of models.

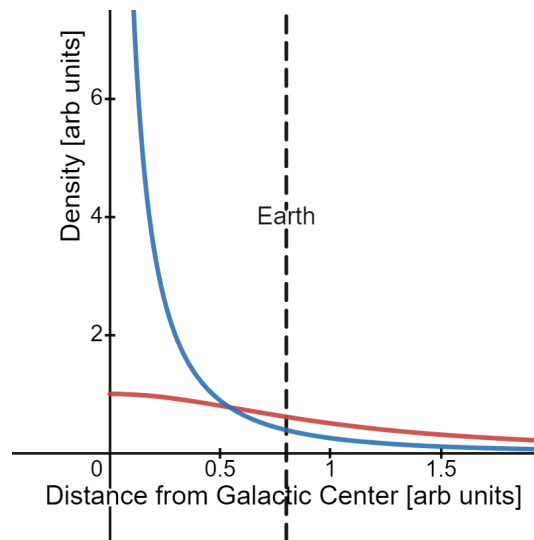


Fig. 4.1 Example of Central Cusp (blue) and Cored Halo (red) density profiles: Navarro-Frenk-White and Isothermal profiles respectively [21]. Dotted line indicates location of Earth on these normalized axes.

Recent review of experimental data tends to support the Cored Halo models, as the DM density at the core certainly must be finite [21]. However, for our needs, we use a combination of both the realistic Cored Halo models and the algebraically simpler Central Cusp models. We begin with the most popular central cusp model, the Navarro-Frenk-White (NFW) profile [34] given below

¹Since photons of different polarizations have different probabilities of gravitational scattering

Table 4.1 Parameters of Dark Matter Halo

| Parameter | Typical Units | SI Units |
|---------------------------|------------------------------------|--|
| Scale DM Density ρ_0 | 840 GeV/cm ³ | 1.35×10^{-1} J/m ³ |
| Local DM Density ρ_l | .387 GeV/cm ³ | 6.20×10^{-5} J/m ³ |
| Number Density n_t | 9×10^{-6} m ⁻³ | 9×10^{-6} m ⁻³ |
| Scale Radius r_0 | 10 kpc | 3.1×10^{20} m |
| Total Radius R | 100 kpc | 3.1×10^{21} m |
| Particle Mass | 10^{14} GeV/c ² | 1.8×10^{-13} kg |

$$\rho(r) = \frac{\rho_0}{\frac{r}{r_s} \left(1 + \frac{r}{r_s}\right)^2}. \quad (4.1)$$

Here, ρ_0 is the experimentally determined scale density and r_s is the scale radius. These parameters are unique for each galaxy, and those of the Milky Way have been studied at length. Notice that at radii $r \gg r_s$, the density $\rho \propto r^{-3}$ as expected. However, to avoid the obvious issue of having infinite density at the core, we artificially impose a maximum density at small radii (to be discussed in more detail later). Table 4.1 outlines some of the relevant parameters to calculate the likelihood of our desired scattering. Note that our choice for the DM particle mass will be explained below. See Refs. [21, 35] for a discussion on reasonable parameter values.

4.1.1 On the Dark Matter Particle Mass

Let us note that there is a general consensus regarding the constant, total mass of the galactic DM halo, determined by astrophysical observations. However, as discussed in the introduction to this paper, the mass of individual DM particles is subject to extensive debate. Certainly, the number density of the DM halo n_t is inversely proportional to the chosen mass of the DM particle. This implies that the luminosity $L = \Phi n_t l$ is inversely proportional to mass. However, from Chapter 3, we recall that the cross section, σ , is directly proportional to the *square* of the target particle mass. Therefore, the scattering yield $J = \sigma L$ is directly proportional to the chosen DM particle mass, as noted in Chapter 3.

Since the desired gravitational interaction is very weak, we are motivated to consider the heaviest models of the DM particle, such as the so-called WIMPzilla models, with masses upward of 10^{14} GeV, popular in string and super-symmetry theories. Selecting such a model will produce the highest rate of scattering, and thus the highest chance of experimentally detecting polarization effects. This result can

be used as a clever way to place upper bounds on the mass of the DM particle. After choosing a certain particle mass, we predict a certain degree of polarization effects. Should an experiment fail to detect predicted polarization effects, we may conclude that we overestimated the DM particle mass, thereby placing a new upper bound on this mass¹. More sensitive instruments can place additional upper limits. Finding such an upper limit would be a significant contribution to this field, as the majority of modern experiments constrain the mass from below, leaving only astrophysical observations to constrain very large DM objects (such as MACHO's as in Ref. [14]), from above. Our technique provides an alternative approach to constrain the mass from above.

4.2 Monte Carlo Simulation

After having introduced the premise and the motivation for choosing the parameters in Tab. 4.1, we now turn to a novel Monte-Carlo simulation to calculate the desired scattering effects, numerically. Our simulation considers a random trajectory from a fixed origin, corresponding to isotropic emission of a photon from the center of the galaxy. Specifically, we randomly select an emission altitude and azimuth (θ_0, ϕ_0) for the photon. We then break the radial trajectory into small pieces. At the end of our first step along the radius, we randomly choose scattering parameters (θ, ϕ) .

Given the (approximately) constant density over the radial step size, and using the cross sections of Chapter 3, we calculate the scattering rate, given these arbitrarily chosen scattering angles. Then using a random "dice throw" we determine whether this scattering event occurs. This "dice throw" consists of two parts: first we randomly choose a scattering angle (ignoring small angle scattering less than 5 degrees) and calculate the scattering yield J , using the cross section and luminosity for a single photon. Next, we randomly choose a number from the range of possible scattering yield values and compare with J to determine whether scattering has taken place. If not, we continue to along the next step of the radius and repeat the above process. If no successful scattering events take place over the total DM halo radius, we proceed to the next photon. Using a sufficiently large number of photons, we thereby simulate the scattering machinery found in Chapter 3. Upon a successful scattering event, using simple geometry, we calculate the eventual location of the photon in an imaginary plane centered around earth (perpendicular to the radial line connecting the Earth and the galactic core). We use histograms to record the photon flux through this plane, centered around Earth.

¹Alternatively, a failure to detect polarization effects could point toward a breakdown of PQG, which formed the basis of our results. Additional research would be needed to conclusively determine the cause of the effect

We begin our simulation with an even number of photons of either linear polarization, which we defined as e^{\parallel} and e^{\perp} . Due to the distinct scattering behavior calculated in Chapter 3, we predict a higher number of scattered photons of a particular polarization over the other. This is reflected on our histograms which record scattered photons in the vicinity of Earth¹, where we used the two different cross sections found in Chapter 3. Our central result is that we expect to detect a higher number of photons of one linear polarization than of the other linear polarization, and this result is reflected in our histograms.

4.2.1 Geometry

Our simulation uses rotation matrices to encode the arbitrary emission and scattering angles, which together define the trajectory of successfully scattered photons. Specifically, we consider conventional axes² and represent the path of a photon using a vector, initially along the positive z -axis. Then, to denote *emission* at angles (θ_0, ϕ_0) , we rotate about the y -axis by θ_0 and rotate about the z -axis by ϕ_0 . After these rotations, we have a new, rotated coordinate system with axes x' , y' , and z' , where the photon trajectory vector is now pointing in the z' direction. The axes (with respect to the old coordinate system) are found using simple geometry

$$x' = \begin{bmatrix} \cos(\phi_0) \\ \sin(\phi_0) \\ -\tan(\theta_0) \end{bmatrix}, y' = \begin{bmatrix} -\sin(\phi_0) \\ \cos(\theta_0) \\ 0 \end{bmatrix}, z' = \begin{bmatrix} \cos(\phi_0)\sin(\theta_0) \\ \sin(\phi_0)\sin(\theta_0) \\ \cos(\theta_0) \end{bmatrix}. \quad (4.2)$$

It can be confirmed that these axes are mutually orthogonal and can be easily normalized. Note, for $\phi_0 > \frac{\pi}{2}$ the components of the x' -axis should change sign to preserve the proper cross-product relationships between the axes according to the right-hand-rule of Calculus.

Now, the photon trajectory vector (now along the z' -axis) will be rotated again, representing *scattering* at angles (θ, ϕ) with respect to the new coordinate system. Specifically, we rotate about the new y' -axis by θ and about the new z' -axis by ϕ . The new orientation of the vector now denotes final trajectory of the photon. See Fig 4.2 for a graphical visualization.

Mathematically, we use the following matrix [36] to rotate about an arbitrary axis V by an angle θ

¹one for either photon polarization

²where we associate the origin with the center of the galaxy, and we place Earth at the coordinates $(R, 0, 0)$

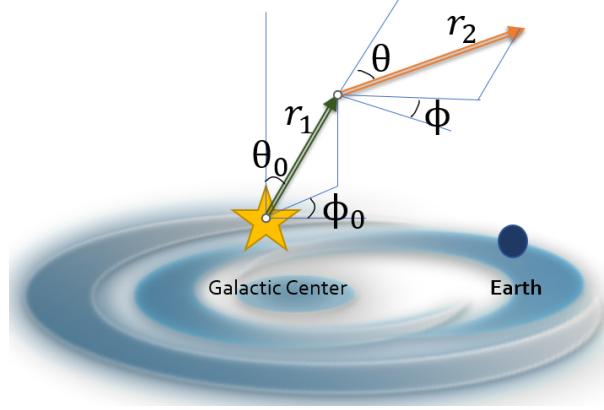


Fig. 4.2 Visualization of the emission and scattering of photon relative to the galactic center and Earth.

$$R(V, \theta) = \begin{bmatrix} V_x^2 + (V_y^2 + V_z^2)\cos(\theta) & V_x V_y(1 - \cos(\theta)) - V_z \sin(\theta) & V_x V_z(1 - \cos(\theta)) - V_y \sin(\theta) \\ V_x V_y(1 - \cos(\theta)) + V_z \sin(\theta) & V_y^2 + (V_x^2 + V_z^2)\cos(\theta) & V_y V_z(1 - \cos(\theta)) - V_x \sin(\theta) \\ V_x V_z(1 - \cos(\theta)) - V_y \sin(\theta) & V_y V_z(1 - \cos(\theta)) + V_x \sin(\theta) & V_z^2 + (V_x^2 + V_y^2)\cos(\theta) \end{bmatrix}. \quad (4.3)$$

Here, the axis of rotation is defined with respect to the original coordinate system $V = (V_x, V_y, V_z)$. In order to describe the final vector, we need only multiply $R(z', \phi) \cdot R(y', \theta) \cdot z' \equiv z''$.

To get the final coordinates of our photon after both emission and scattering, we assume that the photon is emitted along z' over a radial distance r_1 at which point the photon scatters and then travels parallel to z'' over the distance r_2 . This second distance should be long enough such that $r_1 z'_x + r_2 z''_x = R$ which is the distance from the origin (the galactic center) and an imaginary plane centered at $(0,0,R)$ and perpendicular to the x -axis. One might note that we will neglect those photons whose final trajectory points away from this plane. Rearranging, we get $r_2 = (R - r_1 z'_x) / z''_x$.

Our final coordinates are thus simply

$$\begin{aligned} x &= r_1 z'_x + r_2 z''_x, \\ y &= r_1 z'_y + r_2 z''_y, \\ z &= r_1 z'_z + r_2 z''_z. \end{aligned} \quad (4.4)$$

To ensure accuracy of this geometry, we calculated several cross checks of our program. For example, we considered many combinations of emission and scattering angles (assuming the basic case where $r_1 = r_2 = 1$), and calculated the final coordinates with respect to the old coordinate system, and we found the expected scattering behavior. Basic results of this test are included in Appendix D.

4.3 Computational Results

Figure 4.3 below denotes the number of scattered photons that hit an imaginary plane centered around the Earth¹. Each plot records photons of particular linear polarization.

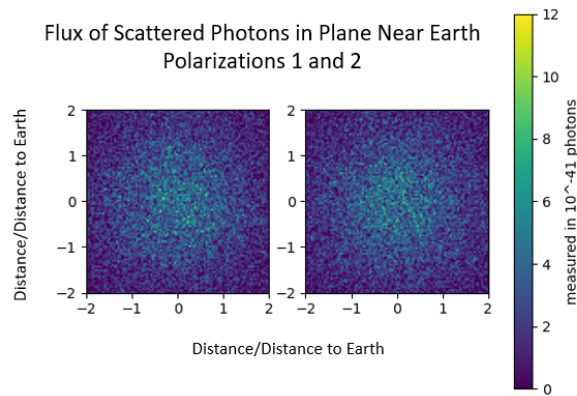


Fig. 4.3 Each ‘hit’ on the histograms represents the final location of an appropriately scattered photon in an imaginary plane centered around Earth. Each histogram records photons of particular linear polarization.

The total photon flux considered here is 10^{51} photons, which is roughly the flux (per second) associated with a large supernova. However, due to the dilute nature of the DM halo and the incredible weakness of gravity (reflected in the small cross section), results are reported as yields per 10^{-41} photons.

Figure 4.4 similarly denotes the number of scattered photons of each polarization, now per unit area (i.e., per m^2) which pass through the above-mentioned plane near Earth. Here, results are reported at the incredibly small scale of 10^{-79} photons. Figure 4.5, our final histogram, records the difference between the number of scattered photons of each polarization. Implications of these results will be further discussed in Chapter 6.

¹perpendicular to the line connecting the Earth and the galactic core

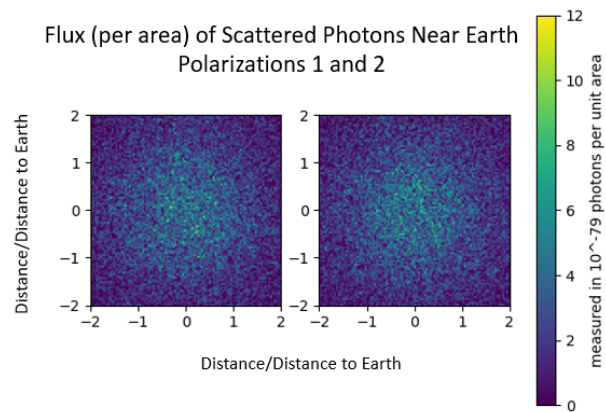


Fig. 4.4 Each 'hit' on the histograms represents the final location of an appropriately scattered photon in an imaginary plane centered around Earth. Results here are reported in number of hits per unit area. Each histogram records photons of particular linear polarization.

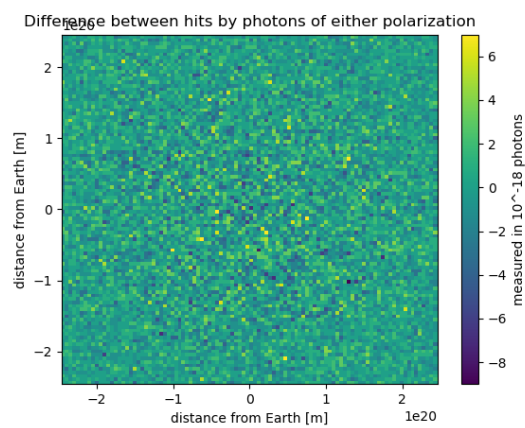


Fig. 4.5 Each 'hit' on the above histogram represents the difference between the number of scattered photons of each polarization at various points on an imaginary plane centered around Earth.

As a quick cross-check, we plot the number of scattering events at each step along the radius of the galactic halo. The resulting histogram matches the normalized NFW profile, as expected. See Fig. 4.6-7 below.

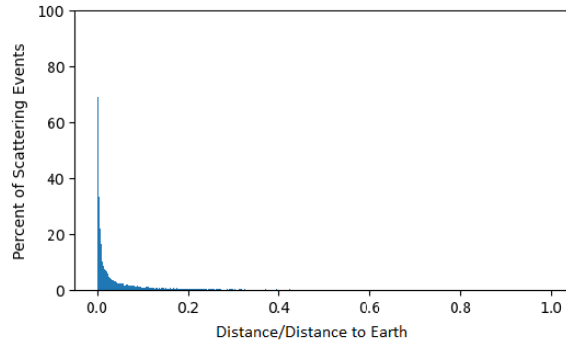


Fig. 4.6 Scattering events vs radius. 10 million photons, log plot.

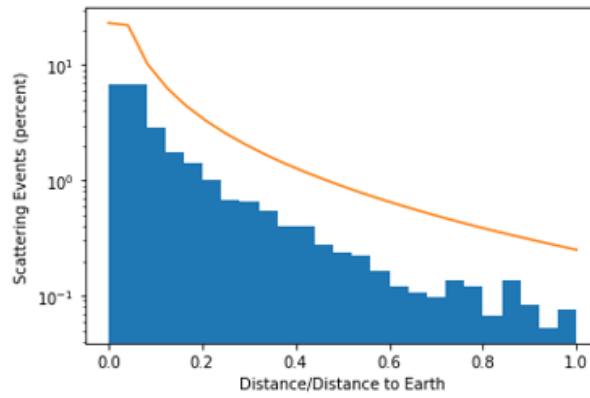


Fig. 4.7 Scattering events vs radius with normalized NFW density profile (orange line). 1 million photons, log plot.

Chapter 5

Applications

5.1 Additional Considerations

In Chapter 3, it is found that the cross section for gravitational photon-scalar scattering is proportional to the constant $\lambda^4/c^6 \approx 3.9 \times 10^{-69}$ in SI units. The weakness of gravity relative to EM interactions is apparent upon a comparison with the coupling constant for electron-muon scattering considered in Appendix B, which is proportional to the square of the fine structure constant $\alpha^2 = \frac{1}{137}$.

We also may note that in the gravity case, the cross section increases in direct proportion with the mass of the target particle. It may be instructive to plot the cross section versus this mass, but we note that even for the heaviest particles ¹, the cross section is still incredibly small. To illustrate this, we calculate the relevant cross sections for scattering over large angles (between 85 and 95 degrees), where we expect the highest polarization dependence. This is shown in Fig. 5.1.

The small size of this cross section arises due to the tiny coupling constant mentioned above. This problem motivated the MC simulation of Chapter 4, where we attempted to compensate by choosing a very large number of target particles over a large distance. Alternatively, we may consider a variety of larger, ‘macroscopic’ targets, which are often approximated as very massive scalar particles (as they carry 0 net spin, see Ref. [37]). However, we admit that this case might stretch the limits of reasonability of the effective field theory discussed in Chapter 2.

¹such as those allowed by supersymmetric theories [35]

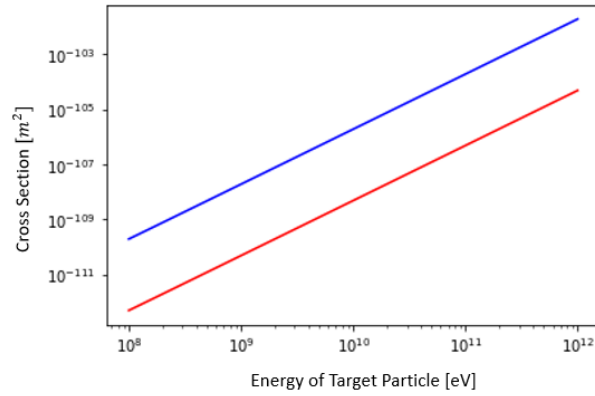


Fig. 5.1 Cross Section for large angle scattering vs mass energy of target, in double log scale. Red and blue curves correspond to photons of each of the two linear polarization states

5.2 Scattering on Macroscopic Targets

Consider a large object, such as the sun, with a fixed mass within a certain radius. Such a target may be easily modeled as a large scalar particle [37]. If a polarized photon scatters on this target, with mass M , at the outer edge of its radius r , classical relativity predicts that the angle of deflection is approximately governed by [38]

$$\theta = \frac{4GM}{rc^2}. \quad (5.1)$$

Here, G is the gravitational constant and c is the speed of light. This angle represents roughly the ‘most common’ scattering angle for the photon. According to the Equivalence Principle of GR, all photons which pass near the Sun at distance r must scatter at this angle. However, as we have seen, the polarization-dependent behavior of photon-scalar scattering will violate this rule [37]. Using the equations of Chapter 3, we can calculate the cross section corresponding to this angle for selected targets. To do this, we only need to integrate the differential cross sections given by Eq. (3.14)-(3.15) over a chosen range of angles.

We consider three astronomical target masses: the Sun, the elliptical galaxy M87, and the supermassive black hole M87*. Choosing the impact parameter as simply the radius of each target, we find that the resulting cross sections indicate very little induced polarization by the scattering, with the exception of scattering near the black hole M87*. Results are included in Table 5.1 on the following page.

Table 5.1 Cross Sections for Typical Bending Angles (according to GR).

| Target Mass | Typical Bending Angle | | Cross Sections | |
|--|------------------------|----------------------|-------------------------------------|-------------------------------------|
| | Radius | θ (radians) | $\sigma_{\parallel\parallel}$ | $\sigma_{\perp\perp}$ |
| 2.0×10^{30} kg (Sun) | 7.0×10^8 m | 8.5×10^{-6} | 6.1×10^{16} m ² | 6.1×10^{16} m ² |
| $6.0 \times 10^{12} * M_{\odot}$ (M87) | 1.5×10^{21} m | 8.9×10^{-6} | 3.0×10^{41} m ² | 3.0×10^{41} m ² |
| $6.5 \times 10^9 * M_{\odot}$ (M87*) | 3.8×10^{14} m | 1.0 | 2.4×10^{25} m ² | 1.5×10^{26} m ² |

As a follow-up test, we calculate the cross sections corresponding to larger-angle scattering (which is certainly possible according to scattering theory, but less likely than the typical bending angle above), we find considerable polarization of the light, summarized in Table 5.2 below, which reports the cross sections integrated between 85 and 95 degrees.

5.2.1 Range of Applicability

Having discussed a variety of application, we must discuss the range of applicability of our equations (i.e., the reasonability of the above predictions). We first recognize that our model is built using Perturbative Quantum Gravity (PQG), which, as discussed in the introduction, is an effective theory of quantum gravity with certain limits. The primary limitation of this model is that the curved space-time metric is assumed to consist of simple perturbations from the flat Minkowski metric. Practically, this would likely preclude discussion of extremely massive objects such as black holes. However, moderately heavy objects (such as the sun or earth) can be described perturbatively, as the local curvature is still relatively small. However, when the total integrated curvature grows large, the predictions will become less accurate [28]. Further, at the Planck energy scale, the "effective" theory breaks down completely [28]. We thus conclude that while scattering on the Sun and M87 are reasonable, as argued in Ref. [37], but scattering on the supermassive M87* is outside the range of applicability of our initial assumptions.

Table 5.2 Cross Sections for Large Bending Angles.

| Target | Cross Sections (large angles) | |
|--------|-------------------------------------|-------------------------------------|
| | $\sigma_{\parallel\parallel}$ | $\sigma_{\perp\perp}$ |
| Sun | 6.1×10^{16} m ² | 6.1×10^{16} m ² |
| M87 | 3.0×10^{41} m ² | 3.0×10^{41} m ² |
| M87* | 2.4×10^{25} m ² | 1.5×10^{26} m ² |

5.3 On the Subject of Entanglement

We next examine another implication of polarization effects in gravitational scattering. Consider high-energy gamma rays, for which the photon polarization has been maximally entangled. Such photons are commonly produced by electron-positron annihilation [39]. Given an entangled pair of such photons, the polarization vectors of each photon are perpendicular to each other [40]. Classically, these polarization vectors are parallel transported during relativistic gravitational lensing [38], and thus we expect the polarization entanglement to be 'intact' after scattering. However, this is not the case when considering quantum effects. Using the polarization-dependent cross sections calculated in Chapter 3, we expect each entangled photon to display distinct scattering behavior. This would be a direct violation of the equivalence principle of GR, which predicts that photons of either polarization would follow the same trajectory [38, 37]. Further, this would mean that the photon entanglement will decohere!

We reflect back to our Monte-Carlo simulation of Chapter 4. The galactic center is a strong source of entangled gamma rays, with over 10^{43} positron annihilation events per second [41]. We are thus motivated to consider scattering of *entangled* photons in the Dark Matter halo of our galaxy. Through the exchange of virtual gravitons with Dark Matter, we expect that photon entanglement will decohere, albeit to only a small degree. This entanglement breaking channel would occur entirely through a quantum gravity effect.

As an important aside, we compare this quantum gravity effect to a related entanglement breaking channel, predicted by Quantum Field Theory (QFT) in curved space-time. This formalism extends ordinary QFT to describe quantum effects on a curved background metric, i.e., under the influence of *classical* gravity (in contrast with the Perturbative Quantum Gravity used in this work, in which gravity itself is also quantized). The literature predicts a wide range of entanglement breaking by gravity in this formalism [26, 27], which we roughly estimate to be orders of magnitude larger than entanglement breaking via graviton exchange. Our effects therefore likely present a small correction to the semi-classical entanglement breaking on QFT in curved space-time (see Ref. [42] for an example of proposed experiment to test entanglement breaking in QFT in curved space-time), and future research will be required to carefully identify the cause of any experimentally observed phenomena.

It may be essential to find a signature of the effects produced by graviton exchange, as reported in this paper. Future research can perhaps be conducted in analogy with Compton scattering of polarized

photons [43, 44]. It has been shown [45, 46, 47] that polarization-dependent Compton scattering can be encoded in a unique matrix representation, which acts on Stokes' vectors representing polarized photons. Current research [48] uses this scattering matrix on the Stokes' vectors denoting entangled photons. See [49] for a good review of this notation. Using the scattering machinery presented in Chapter 3, we are able to build an analogous matrix encoding the polarization effects of our photon-scalar gravitational scattering. This 3×3 matrix acts on Stokes' vectors and predicts the quantum state of the entangled pair after scattering. Using traditional quantum mechanics, the precise degree of entanglement breaking can be calculated.

Previous research [33] has considered a similar interaction in PQG: graviton exchange between two entangled photons. This light-by-light gravitational scattering is predicted to decohere the entanglement of the photon pair. We now suggest that photon-scalar scattering would have this same effect. This would be a novel implication, as we continue to build the case that entanglement decoherence can be indirect evidence for the existence of gravitons, see Ref. [50] for a similar experiment. We note that experimentally, our photon-scalar scattering may be more reasonable than photon-photon scattering, which is dominated by interfering electromagnetic effects.

Chapter 6

Analysis

6.1 Polarization Effects of Photon Scattering

From the results in Chapters 3-5, we may now analyze the expected polarization effects in graviton-mediated photon-scalar scattering. Results from Chapter 3 are clear that some polarization effects are expected, although the tiny coupling constant indicates that this effect will be very small in most cases. In Chapter 4, we attempted to overcome the weakness of the effect by using a very large collection of target particles, over a large distance, specifically, examining gravitational scattering of light on the Dark Matter halo of the Milky Way galaxy. From the resulting histograms which denote the scattered photons which pass through a region near earth, it is clear that photons of one polarization will scatter more often than photons of the other polarization. However, the small pre-factor indicates, that even for a large number of photons, comparable to a very luminous supernova, there are simply not enough photons which reach Earth to be detected.

As possible work-arounds for this challenge, we are free to run the simulation under new parameters. Specifically, we can consider a larger photon flux, perhaps corresponding to an ultra-luminous quasar, which are referred to as the brightest objects in the universe. We can also expand our choice for DM mass, by choosing some form of highly exotic matter, such as topological defects, quantum black holes, etc, whose masses are far larger than the WIMP-zilla mass chosen here [51]. With these changes, it may in fact be feasible to detect the scattered photons (of both polarizations) here on Earth. The results from such a test are displayed in Appendix D.

Scattering on a macroscopic targets in Chapter 5 also leads to some interesting results. We found that the desired polarization effects are large enough to be observed, although we relied heavily on

some classical assumptions and in one case, perhaps exceeded the range of applicability of PQG. Despite these limitations, the desired effect may still be found.

It may be advantageous to consider recent stunning advancements in observational astronomy. In 2021, for the first time, using the enormously successful Event Horizon Telescope (EHT) astronomers detected polarization of photons around supermassive black holes [52]. Certainly a wide variety of effects are behind light polarization, but we note that if similar observations around other macroscopic targets yield polarization, which cannot be explained by other forces, we could support the hypothesis that gravity too has polarizing properties, due to exchange of gravitons.

6.2 Additional Applications

It may be beneficial to point out that the Monte-Carlo simulation used to calculate gravitational scattering on Dark Matter can be modified for other purposes. Specifically, current research has suggested novel light-quark models for Dark Matter, notably the $d^*(2380)$ hexaquark, which is expected to interact with light in predictable ways [53]. In order to test this hypothesis, we are free to substitute the parameters¹ for the desired interactions. Our code is versatile enough to be convenient for such modifications.

¹cross sections, densities, etc.

Chapter 7

Conclusions

7.1 Discussion

7.1.1 Impact on Quantum Gravity

In our discussion of photon-scalar scattering via graviton exchange, we build on previous research on the exchange of gravitons between elementary particle of different spin, such as [54]. In our research, we find polarization dependence in gravitational deflection of light. This polarization dependence is a purely quantum effect, similar to the tiny quantum corrections to the gravitational potential in Refs. [12, 28]. Such a scenario is a violation of the equivalence principle of GR [38], and if detected, provides convincing evidence for a field-theoretic description of gravity. In other words, this effect would highly suggest the existence of gravitons as the mediator of the gravitational force.

7.1.2 Impact of Dark Matter Research

Our application to Dark Matter is also highly suggestive. Our results from the Monte-Carlo simulation predict that galactic photons will become polarized by the Dark Matter Halo of the Milky Way, although the effect is small. This polarization dependence is directly proportional to the mass of the Dark Matter particle¹. A wide range of Dark Matter particle masses are predicted by the literature, from a fraction of an eV to ultra-heavy WIMPzilla particles $\geq 10^{14}$ GeV [13] to primordial black holes with masses upward of 1000 solar masses [51]. Our predictions may thus be theoretically useful as a method to bound the Dark Matter particle mass from above, which would complement the usual

¹or any other chosen scattering target

methods of bounding this mass from below. As mentioned in Chapter 4, it would be vital to determine that the fault does not lie with PQG to conclusively set this upper bound for the DM particle mass.

We must recognize that our calculations considered a very strong source of *linearly* polarized photons. Such linear polarization is reasonable as ordinary radiation from the galactic core can become plane polarized by an anisotropic process, such as scattering by interstellar dust or from stellar sources [22]. However, the predicted quantum-gravity effect considered is very small, even restricting our attention to extremely luminous events, such as supernovae, gamma-ray bursts, and quasars. Our alternative option is to consider macroscopic targets as in Chapter 5, although we must ensure that we do not overstep the range of applicability of our effective field theory of gravity

7.1.3 Entanglement Breaking

As seen in our research, the polarization of photons can be used as an entanglement breaking channel. Further research is planned by the author to investigate the degree of entanglement decoherence after the scattering of entangled photons in the Dark Matter Halo, given a diverse range of Dark Matter models. This entanglement breaking could be measured by a detector at earth and can be further evidence for the quantum effects of gravity and serve to bound the mass of the hypothesized Dark Matter particle.

Bibliography

- [1] Sheldon Lee Glashow. “Towards a unified theory: Threads in a tapestry”. In: *Reviews of Modern Physics* 52.3 (1980), p. 539.
- [2] J Schwinger. “Quantum electrodynamics-An individual view”. In: *Le Journal de Physique Colloques* 43.C8 (1982), pp. C8–409.
- [3] Abdus Salam. “The electroweak force, grand unification and superunification”. In: *Physica Scripta* 20.2 (1979), p. 216.
- [4] William Marciano and Heinz Pagels. “Quantum chromodynamics”. In: *Physics Reports* 36.3 (1978), pp. 137–276.
- [5] Enrique Alvarez. “Quantum gravity: an introduction to some recent results”. In: *Reviews of Modern Physics* 61.3 (1989), p. 561.
- [6] Robert M Wald. *General relativity*. University of Chicago press, 1984.
- [7] David J Griffiths and Darrell F Schroeter. *Introduction to quantum mechanics*. Cambridge university press, 2018.
- [8] Abraham Pais. “Einstein and the quantum theory”. In: *Reviews of modern physics* 51.4 (1979), p. 863.
- [9] David Prinz. “Gravity-matter Feynman rules for any valence”. In: *Classical and Quantum Gravity* 38.21 (2021), p. 215003.
- [10] Zvi Bern. “Perturbative quantum gravity and its relation to gauge theory”. In: *Living Reviews in Relativity* 5.1 (2002), pp. 1–57.
- [11] S Deser, P Van Nieuwenhuizen, and D Boulware. “Uniqueness and nonrenormalizability of quantum gravitation”. In: *General Relativity and Gravitation* (1975), pp. 1–18.
- [12] NEJ Bjerrum-Bohr et al. “Bending of light in quantum gravity”. In: *Physical review letters* 114.6 (2015), p. 061301.
- [13] Manuel Drees and Gilles Gerbier. “Mini–review of dark matter: 2012”. In: *arXiv preprint arXiv:1204.2373* (2012).
- [14] DP Bennett et al. “The MACHO project dark matter search”. In: *Arxiv preprint astro-ph/9510104* (1995).
- [15] Leanne D Duffy and Karl Van Bibber. “Axions as dark matter particles”. In: *New Journal of Physics* 11.10 (2009), p. 105008.
- [16] Leszek Roszkowski, Enrico Maria Sessolo, and Sebastian Trojanowski. “WIMP dark matter candidates and searches—current status and future prospects”. In: *Reports on Progress in Physics* 81.6 (2018), p. 066201.
- [17] Leszek Roszkowski. “Non-baryonic dark matter—a theoretical perspective”. In: *AIP Conference Proceedings*. Vol. 478. 1. American Institute of Physics. 1999, pp. 316–324.

- [18] Hsin-Chia Cheng, Jonathan L Feng, and Konstantin T Matchev. “Kaluza-Klein dark matter”. In: *Physical review letters* 89.21 (2002), p. 211301.
- [19] Paolo Gondolo, Pearl Sandick, and Barmak Shams Es Haghi. “Effects of primordial black holes on dark matter models”. In: *Physical Review D* 102.9 (2020), p. 095018.
- [20] Hitoshi Murayama and Jing Shu. “Topological dark matter”. In: *Physics Letters B* 686.2-3 (2010), pp. 162–165.
- [21] Yoshiaki Sofue. “Rotation curve of the Milky Way and the dark matter density”. In: *Galaxies* 8.2 (2020), p. 37.
- [22] DH Wilkinson. “LXII. A source of plane-polarized gamma-rays of variable energy above 5· 5 mev”. In: *The London, Edinburgh, and Dublin Philosophical Magazine and Journal of Science* 43.341 (1952), pp. 659–662.
- [23] D Boccaletti et al. “Photon-photon scattering and photon-scalar particle scattering via gravitational interaction (one-graviton exchange) and comparison of the processes between classical (general-relativistic) theory and the quantum linearized field theory”. In: *Il Nuovo Cimento B (1965-1970)* 60.2 (1969), pp. 320–330.
- [24] Frederick Gordon Peet. “Cross-sections for the gravitational scattering of massless particles”. PhD thesis. University of British Columbia, 1970.
- [25] VV Skobelev. “Graviton-photon interaction”. In: *Soviet Physics Journal* 18.1 (1975), pp. 62–65.
- [26] Timothy C Ralph, Gerard J Milburn, and T Downes. “Quantum connectivity of space-time and gravitationally induced decorrelation of entanglement”. In: *Physical Review A* 79.2 (2009), p. 022121.
- [27] David Edward Bruschi et al. “Spacetime effects on satellite-based quantum communications”. In: *Physical Review D* 90.4 (2014), p. 045041.
- [28] John F Donoghue. “The effective field theory treatment of quantum gravity”. In: *AIP Conference Proceedings*. Vol. 1483. 1. American Institute of Physics. 2012, pp. 73–94.
- [29] Anthony Zee. *Quantum field theory in a nutshell*. Vol. 7. Princeton university press, 2010.
- [30] W Cordeiro dos Santos. “Introduction to Einstein–Maxwell equations and the Rainich conditions”. In: *arXiv preprint arXiv:1606.08527* (2016).
- [31] Steven Weinberg. “Feynman rules for any spin”. In: *Physical Review* 133.5B (1964), B1318.
- [32] Steven Weinberg. “Feynman rules for any spin. II. Massless particles”. In: *Physical Review* 134.4B (1964), B882.
- [33] Dennis Rätzel, Martin Wilkens, and Ralf Menzel. “The effect of entanglement in gravitational photon-photon scattering”. In: *EPL (Europhysics Letters)* 115.5 (2016), p. 51002.
- [34] Julio F Navarro, Carlos S Frenk, and Simon DM White. “A universal density profile from hierarchical clustering”. In: *The Astrophysical Journal* 490.2 (1997), p. 493.
- [35] Houri Ziaee pour. “A Decaying ultra heavy dark matter (WIMPZILLA): Review of recent progress”. In: *arXiv preprint astro-ph/0005299* (2000).
- [36] Ian R Cole. “Modelling CPV.” PhD thesis. Loughborough University, 2015.
- [37] Huan-Hang Chi. “Graviton bending in quantum gravity from one-loop amplitudes”. In: *Physical Review D* 99.12 (2019), p. 126008.
- [38] Christopher R Burns. *Gravitational lensing of polarized sources*. Bibliothèque nationale du Canada, Ottawa, 2003.

-
- [39] Isabelle Gauthier and Margaret Hawton. “Photon correlations in positron annihilation”. In: *Physical Review A* 81.6 (2010), p. 062121.
- [40] MHL Pryce and JC Ward. “Angular correlation effects with annihilation radiation”. In: *Nature* 160.4065 (1947), pp. 435–435.
- [41] Thomas Siegert et al. “Gamma-ray spectroscopy of positron annihilation in the Milky Way”. In: *Astronomy & Astrophysics* 586 (2016), A84.
- [42] Siddarth Koduru Joshi et al. “Space QUEST mission proposal: experimentally testing decoherence due to gravity”. In: *New Journal of Physics* 20.6 (2018), p. 063016.
- [43] FW Lipps and HA Tolhoek. “Polarization phenomena of electrons and photons. I: General method and application to Compton scattering”. In: *Physica* 20.1-6 (1954), pp. 85–98.
- [44] FW Lipps and HA Tolhoek. “Polarization phenomena of electrons and photons. II: Results for Compton scattering”. In: *Physica* 20.1-6 (1954), pp. 395–405.
- [45] A Wightman. “Note on polarization effects in Compton scattering”. In: *Physical Review* 74.12 (1948), p. 1813.
- [46] Ugo Fano. “Description of states in quantum mechanics by density matrix and operator techniques”. In: *Reviews of modern physics* 29.1 (1957), p. 74.
- [47] William H McMaster. “Matrix representation of polarization”. In: *Reviews of modern physics* 33.1 (1961), p. 8.
- [48] Peter Caradonna et al. “Probing entanglement in Compton interactions”. In: *Journal of Physics Communications* 3.10 (2019), p. 105005.
- [49] Keiichi Edamatsu. “Entangled photons: generation, observation, and characterization”. In: *Japanese Journal of Applied Physics* 46.11R (2007), p. 7175.
- [50] Sugumi Kanno, Jiro Soda, and Junsei Tokuda. “Indirect detection of gravitons through quantum entanglement”. In: *Physical Review D* 104.8 (2021), p. 083516.
- [51] Bernard Carr, Florian Kühnel, and Marit Sandstad. “Primordial black holes as dark matter”. In: *Physical Review D* 94.8 (2016), p. 083504.
- [52] Kazunori Akiyama et al. “First M87 event horizon telescope results. VII. Polarization of the ring”. In: *The Astrophysical Journal Letters* 910.1 (2021), p. L12.
- [53] M Bashkanov and DP Watts. “A new possibility for light-quark dark matter”. In: *Journal of Physics G: Nuclear and Particle Physics* 47.3 (2020), 03LT01.
- [54] Bruce M Barker, Suraj N Gupta, and Richard D Haracz. “One-graviton exchange interaction of elementary particles”. In: *Physical Review* 149.4 (1966), p. 1027.
- [55] F Hautmann. “An Introduction to QED & QCD”. In: *RAL High Energy Physics Summer School* (2012).

Appendix A

Conventions

Einstein Summation Convention

This convention is simply a convenient notation used to denote implicit summation over indexed terms in an expression. In the following pages, Latin indices take the values 1,2,3 whereas Greek indices take the values 0,1,2,3.

Tensors

Variables may be given one or more indices. If a variable carries no index, it is called a rank 0 tensor, and it represents a scalar quantity. If a variable carries a single index, it is called a rank 1 tensor and it is represented by a vector. For example, consider the 4-momentum $k^\mu = (k^0, k^i) = (k^0, k^1, k^2, k^3)$ where k^0 is the relativistic energy and k^i denotes the spatial components of momentum.

Note: a vector quantity will never carry more than a single index. If a vector ever appears to carry multiple indices, then the extra subscript or superscript is actually a *label*, not an index. For example, when describing momentum of a particle, we may use k_1^μ and k_2^μ . The subscripts 1 and 2 are simply labels, which perhaps refer to initial and final momentum, respectively. Diagrams and in-text comments will explain any potential ambiguity as needed.

If a variable does carry 2 indices, such as $\eta_{\mu\nu}$, $g_{\mu\nu}$, or $h_{\mu\nu}$, then it is a rank 2 tensor and is characterized by a 3×3 or 4×4 matrix (depending on whether the indices are Latin or Greek).

Summation

Traditionally, when taking the dot product of two vectors, we use the formula

$$\sum_{i=1}^3 a_i b^i = a_1 b^1 + a_2 b^2 + a_3 b^3. \quad (\text{A.1})$$

Notice that the index i is present once in the lower position and once in the upper position. The result of the summation is a scalar quantity. In the Einstein notation, we omit the cumbersome sigma notation and simply write

$$a_i b^i = a_1 b^1 + a_2 b^2 + a_3 b^3, \quad (\text{A.2})$$

where the repetition of the index i (once downstairs and once upstairs) implies summation over all possible values of i . Notice that by summing, the index disappears and is not present on the right hand side of the equation

Now, the product of rank 2 tensors will behave similarly. For example, in chapter 2, just prior to Eq. 2.14, we use the expression

$$\sqrt{-g} \approx 1 + \frac{\kappa}{2} \eta_{\alpha\beta} h^{\alpha\beta}. \quad (\text{A.3})$$

Now, the tensor product on the right hand side of this equation includes repetition of the indices α and β , which implies summation. As with the dot product of vectors, the result of this summation is a scalar. Notice the left hand side is also a scalar quantity (as expected), see Chapter 2 for details.

Example

To determine which indices are summed in an equation which has many indices, there are a couple of basic rules. If a single term of an equation contains a repeated index (once in the upper position, and once in the lower position), then we must sum over all index values. However, if an index appears only once in a term, then there is no summation. For example consider the equation

$$F^{ij} = \eta^{ik} \eta^{jl} F_{kl}. \quad (\text{A.4})$$

Notice that the term on the right hand side repeats the indices k and l , which each appear in the upper and lower position of tensors. We thus sum over all values of k and l , and these indices subsequently vanish. In contrast, the indices i and j are only present once per term, in the upper position (and there is no corresponding tensor which carries those indices in the lower position), and hence they are not summed.

It is important that all terms carry identical unsummed indices. For example, the equation $a^i = b_j c^j$ makes no sense, because we have an unsummed index on the left, but only summed indices on the right (i.e., a scalar product of vectors)¹. Compare with a better equation $a^i = d^i (b_j c^j)$. Here, the unsummed indices are consistent on the left and right (i.e., there is a vector quantity on both sides of this equation).

Raising and Lowering Indices

It is important that summed indices appear once upstairs and once downstairs. In many cases it is necessary to raise or lower indices to correctly contract the indices. Given a tensor $T_{\mu\nu}$, we may raise the indices using a metric tensor as follows

$$\begin{aligned} T^{\alpha\beta} &= g^{\alpha\mu} T_{\mu}^{\beta} = g^{\alpha\mu} g^{\beta\nu} T_{\mu\nu}, \\ T_{\alpha\beta} &= g_{\alpha\mu} T_{\beta}^{\mu} = g_{\alpha\mu} g_{\beta\nu} T^{\mu\nu}. \end{aligned} \tag{A.5}$$

We shall frequently perform this manipulation using the Minkowski metric $\eta_{\mu\nu}$, which is simply the 4×4 matrix with zeros everywhere except the diagonal, and $\text{diag}(\eta_{\mu\nu}) = (+1, -1, -1, -1)$.

Note: The indices themselves are merely 'dummy variables' and may be interchanged for new symbols, provided that each term will contain at most two occurrences of each index (otherwise, we would encounter ambiguity on which tensors are contracted with each other).

Summary

In summary, tensors may have 0,1,2 or more indices, and repeated indices in a particular term (with one downstairs and one upstairs) are implicitly summed. Non-repeated indices, in contrast, are not summed. An index can appear at most twice in any term of an equation, and each term must

¹In other words, we have a vector on the left and a scalar on the right

contain identical unsummed indices. Indices of a tensor can also be raised or lowered by contracting with the metric tensor, as needed.

Other

In this thesis, certain equations may use natural units where $h = c = 1$. In all cases, Planck's Constant and the speed of light are restored prior to conversion to SI units (unless otherwise stated).

Kronecker Delta

We define the Kronecker delta

$$\delta^{\rho\sigma} = \begin{cases} 1 & \text{if } \rho = \sigma \\ 0 & \text{if } \rho \neq \sigma \end{cases}. \quad (\text{A.6})$$

Immediately from the definition, we know that the Kronecker is symmetric $\delta^{\rho\sigma} = \delta^{\sigma\rho}$. Also we can derive that $\delta^{\rho\sigma}\delta_{\sigma\tau} = \delta^{\rho\tau}$. An immediate implication is that

$$\delta^{\rho\sigma}\delta_{\sigma\rho} = \delta^{\rho\rho} = \delta^{00} + \delta^{11} + \delta^{22} + \delta^{33} = 1 + 1 + 1 + 1 = 4, \quad (\text{A.7})$$

where the repeated index ρ implies summation over all possible values of ρ . This fact is used to derive Eq. 3.9

Symmetrization

Very often, there are underlying symmetries behind indices used. With that in mind, we let $A_{(\rho}B_{\sigma)}$ denote symmetrization with respect to the indices ρ and σ . More precisely

$$A_{(\rho}B_{\sigma)} = \frac{1}{2}(A_{\rho}B_{\sigma} + A_{\sigma}B_{\rho}). \quad (\text{A.8})$$

This abbreviation is used throughout Chapter 3.

Mandelstam Variables

In two body scattering $p_1 + p_2 \rightarrow p_3 + p_4$ it is often convenient to write the scattering machinery in terms of Mandelstam variables, which are quantities which encode the 4-momenta of particles in a Lorentz-invariant way. The variables can be defined as follows

$$\begin{aligned} s &= (p_1 + p_2)^2 = (p_3 + p_4)^2, \\ t &= (p_1 - p_3)^2 = (p_2 - p_4)^2, \\ u &= (p_1 - p_4)^2 = (p_2 - p_3)^2, \end{aligned} \tag{A.9}$$

where p_1, p_2 and p_3, p_4 are the 4-momenta of the ingoing and outgoing particles respectively. Notice that we drop the indices for readability. Now, if we use m_i to denote the mass of the particle with momentum p_i , we get the property

$$s + t + u = m_1^2 + m_2^2 + m_3^2 + m_4^2. \tag{A.10}$$

We can further derive that

$$\begin{aligned} (p_1 \cdot p_2) &= (p_2 \cdot p_4) = (s - m_1^2 - m_2^2)/2 \\ -(p_1 \cdot p_3) &= -(p_2 \cdot p_4) = (m_1^2 + m_3^2 - t)/2 \\ -(p_1 \cdot p_4) &= -(p_2 \cdot p_3) = (m_1^2 + m_4^2 - u)/2. \end{aligned} \tag{A.11}$$

Appendix B

Parallel with Electromagnetism

In Chapter 3 we discussed the matrix elements for lowest order diagram for electron-muon scattering

$$i\mathcal{M} = ie\bar{u}(s_c, p_c)\gamma^\mu u(s_a, p_a) \frac{-ig_{\mu\nu}}{q^2 + i\epsilon} ie\bar{u}(s_d, p_d)\gamma^\nu u(s_b, p_b). \quad (\text{B.1})$$

We now derive additional machinery for this important QED example for comparison with the analogous gravity case.

Complex Conjugation of the "Spinor Sandwich"

We know that our cross section will eventually involve the square of the modulus of our scattering amplitude (i.e. $|\mathcal{M}|^2$). Hence, we need to find the complex conjugate of our amplitude. Now, we focus on the "spinor sandwich" i.e. the $\bar{u}(p_b)\gamma^\mu u(p_a)$ factors in the amplitude. Notice we temporarily drop the spin labels for brevity.

From our definitions of our gamma matrices, we can easily verify the relationships $(\gamma^\mu)^\dagger = \gamma^0\gamma^\mu\gamma^0$, $\gamma^0\gamma^{\mu\dagger}\gamma^0 = \gamma^\mu$, and $(\gamma^0)^2 = +1$, and. Hence, we calculate¹

$$\begin{aligned} [\bar{u}(p_b)\gamma^\mu u(p_a)]^* &= [\bar{u}(p_b)\gamma^\mu u(p_a)]^\dagger = [u^\dagger(p_b)\gamma^0\gamma^\mu u(p_a)]^\dagger = \\ &= [u^\dagger(p_a)\gamma^{\mu\dagger}\gamma^0 u(p_b)] = [u^\dagger(p_a)\gamma^0\gamma^0\gamma^{\mu\dagger}\gamma^0 u(p_b)] = [\bar{u}(p_a)\gamma^\mu u(p_b)]. \end{aligned} \quad (\text{B.2})$$

¹By recognizing that our "spinor sandwich" is nothing more than a Lorentz scalar, we know that the complex conjugate is the same as the Hermitian conjugate.

In general, we find that taking the complex conjugate of $\bar{u}(p_b)\gamma^\mu \dots \gamma^\nu u(p_a)$ reverses the order of our gamma matrices and exchanges the two spinors, eventually giving $\bar{u}(p_a)\gamma^\nu \dots \gamma^\mu u(p_b)$.

Toward the Cross Section

From the above section, we calculate

$$\begin{aligned} |\mathcal{M}|^2 &= \frac{e^4}{q^4} [\bar{u}(p_c)\gamma^\mu u(p_a)\bar{u}(p_d)\gamma_\nu u(p_b)] [\bar{u}(p_a)\gamma^\nu u(p_c)\bar{u}(p_b)\gamma_\mu u(p_d)] \\ &= \frac{e^4}{q^4} [\bar{u}(p_c)\gamma^\mu u(p_a)\bar{u}(p_a)\gamma^\nu u(p_c)] [\bar{u}(p_b)\gamma_\mu u(p_d)\bar{u}(p_d)\gamma_\nu u(p_b)]. \end{aligned} \quad (\text{B.3})$$

We will first consider initially unpolarized electrons. We thus average over initial spins and sum over final spins using

$$\begin{aligned} \frac{1}{4} \sum_{spins} |\mathcal{M}|^2 &= \frac{e^4}{4q^4} \sum_{s_a} \sum_{s_c} [\bar{u}(p_c)\gamma^\mu u(p_a)\bar{u}(p_a)\gamma^\nu u(p_c)] \sum_{s_b} \sum_{s_d} [\bar{u}(p_b)\gamma_\mu u(p_d)\bar{u}(p_d)\gamma_\nu u(p_b)] \\ &\equiv \frac{e^4}{4q^4} L^{\mu\nu} M_{\mu\nu}. \end{aligned} \quad (\text{B.4})$$

The factor of 1/4 arises because we are averaging over initial spins (and we consider 4 initial spin states). Also, we implicitly define the Lepton tensors $L^{\mu\nu}$ and $M_{\mu\nu}$ for the electron and muon respectively. Notice that we can now use the completeness relations (to be derived shortly) which gives

$$\begin{aligned} L^{\mu\nu} &= Tr(\gamma^\mu(\not{p}_a + m_e)\gamma^\nu(\not{p}_c + m_e)), \\ M_{\mu\nu} &= Tr(\gamma_\mu(\not{p}_d - M)\gamma_\nu(\not{p}_d - M)), \end{aligned} \quad (\text{B.5})$$

where M is the mass of the muon. Because our gamma matrices satisfy the anti-commutation relation $\{\gamma^\mu, \gamma^\nu\} = 2\eta^{\mu\nu}$, there exist convenient formulas to evaluate the traces of products of gamma matrices. Using these relations, we get

$$\begin{aligned}
L^{\mu\nu} &= 4(p_a^\mu p_c^\nu + p_a^\nu p_c^\mu - \eta^{\mu\nu} p_a \cdot p_c) + 4\eta^{\mu\nu} m_e^2, \\
M_{\mu\nu} &= 4(p_{\mu b} p_{\nu d} + p_{\nu b} p_{\mu d} - \eta_{\mu\nu} p_b \cdot p_d) + 4\eta_{\mu\nu} M^2.
\end{aligned} \tag{B.6}$$

Now, we put these together to obtain

$$\begin{aligned}
&\frac{1}{4} \sum_{spins} |\mathcal{M}|^2 \\
&= \frac{e^4}{4q^4} \times 4 [p_a^\mu p_c^\nu + p_a^\nu p_c^\mu + (m_e^2 - p_a \cdot p_c) \eta^{\mu\nu}] \times 4 [p_{\mu b} p_{\nu d} + p_{\nu b} p_{\mu d} + (M^2 - p_b \cdot p_d) \eta_{\mu\nu}] \\
&= \frac{4e^4}{q^4} [2(p_a \cdot p_b)(p_c \cdot p_d) + 2(p_a \cdot p_d)(p_c \cdot p_b) + 2(p_a \cdot p_c)(M^2 - p_b \cdot p_d) + 2(p_b \cdot p_d)(m_e^2 - p_a \cdot p_c) \\
&\quad + 4(M^2 - p_b \cdot p_d)(m_e^2 - p_a \cdot p_c)] \\
&= \frac{4e^4}{q^4} [2(p_a \cdot p_b)(p_c \cdot p_d) + 2(p_a \cdot p_d)(p_c \cdot p_b) - 2(p_a \cdot p_c)M^2 - 2(p_b \cdot p_d)m_e^2 + 4m_e^2 M^2]. \tag{B.7}
\end{aligned}$$

Now, to make this expression more concise, we can express the momenta in terms of the Mandelstam variables where we use the fact that $p_a^2 = p_c^2 = m_e^2$ and $p_b^2 = p_d^2 = M^2$. Then, we get the exact answer

$$\frac{1}{4} \sum_{spins} |\mathcal{M}|^2 = \frac{2e^4}{t^2} [s^2 + u^2 + 4(m_e^2 + M^2)(s + u) + 6(m_e^2 + M^2)^2]. \tag{B.8}$$

The Cross Section (High Energy Limit)

Returning to Figure 1., we can describe each 4-momentum in the center of mass frame, in the high energy limit $E \gg m_e, M$, as follows

$$\begin{aligned}
p_a &= (E, 0, 0, E), \\
p_b &= (E, 0, 0, -E), \\
p_c &= (E, E \sin(\theta), 0, E \cos(\theta)), \\
p_d &= (E, -E \sin(\theta), 0, -E \cos(\theta)).
\end{aligned} \tag{B.9}$$

This leads to the high energy approximations

$$\begin{aligned}
s &\approx 2(p_a \cdot p_b)^2 = 2(p_c \cdot p_d)^2 = 4E^2 \\
t &\approx -2(p_a \cdot p_c)^2 = -2(p_b \cdot p_d)^2 = -2E^2(1 - \cos(\theta)) \\
u &\approx -2(p_a \cdot p_d)^2 = -2(p_b \cdot p_c)^2 = -2E^2(1 + \cos(\theta)).
\end{aligned}$$

In this limit, we can ignore m_e and M , and plugging into Eq. B.10, we get that

$$|\mathcal{M}|^2 = 8e^4 \frac{1 + \frac{1}{4}(1 + \cos(\theta))^2}{(1 - \cos(\theta))^2}. \quad (\text{B.10})$$

We now recall the formula for the cross-section for $p_a + p_b \rightarrow p_c + p_d$ scattering in the center of mass frame [55]

$$\frac{d\sigma}{d\Omega} = \frac{1}{64\pi^2 W^2} \frac{|p_c|}{|p_a|} |\mathcal{M}|^2, \quad (\text{B.11})$$

where $W^2 = (p_a + p_b)^2 = (2E)^2$ denotes the square of the total energy of the system (in CoM frame) and is equivalent to our Mandelestam variable s . Now, simply plugging into this formula, we get¹

$$\frac{d\sigma}{d\Omega} = \frac{e^4}{8\pi^2 (2E)^2} \frac{1 + \frac{1}{4}(1 + \cos(\theta))^2}{(1 - \cos(\theta))^2}. \quad (\text{B.12})$$

Additional Approximations

Now, with the above framework in place, we are able to consider electron-muon scattering under additional approximations.

Muon Mass Very Large

At around 106 MeV, the muon rest mass is over 200 times that of the electron. Nonetheless, during the scattering, the muon should experience some small recoil. However, in a new approximation, we shall suppose our muon is extremely massive and will thus have no recoil at all. Our goal is to better understand how our revised differential cross section should behave.

¹Notice we approximate $\frac{|p_c|}{|p_a|} \approx 1$

Cross Section (No Recoil)

In the limit that $M/m_e \rightarrow \infty$ we can use for the muon the spinors for a particle at rest, i.e.

$$\begin{aligned}\bar{u}(p_b)\gamma^i u(p_d) &\approx 0, \\ \bar{u}(p_b)\gamma^0 u(p_d) &\approx 1,\end{aligned}\tag{B.13}$$

so that our new scattering amplitude becomes

$$\mathcal{M} = \frac{-ie^2}{q^2} \bar{u}(p_a)\gamma^0 u(p_c).\tag{B.14}$$

Hence, averaging over initial spins gives

$$\frac{1}{4} \sum_{spins} |\mathcal{M}|^2 = \frac{e^4}{4q^4} \sum_{spins} [\bar{u}(p_a)\gamma^0 u(p_c)][\bar{u}(p_c)\gamma^0 u(p_a)] = \frac{e^4}{4q^4} \text{Tr}(\gamma^0(\not{p}_a - m_e)\gamma^0(\not{p}_c - m_e)).\tag{B.15}$$

Suppose we neglect the mass of the electron and note that the trace is invariant under cyclic permutations. Then, moving around the terms and noting $\gamma^0\gamma^0 = I$, we find

$$\frac{1}{4} \sum_{spins} |\mathcal{M}|^2 = \frac{4e^4}{q^4} (p_a \cdot p_b).\tag{B.16}$$

Whereas before we approximated $s \approx 2(p_a \cdot p_b)$ in the relativistic limit, we now must consider large M , so we must write $(p_a \cdot p_c) \approx (s - M^2)/2$ and so on. Hence, our expression above becomes

$$= \frac{2e^4 s^2}{t^2} (s - M^2).$$

Now this leads to the relatively simple cross section

$$\frac{d\sigma}{d\Omega} = \frac{e^4}{64\pi^2 s} \frac{(s - M^2)}{t^2},\tag{B.17}$$

where we denote the heavy muon mass as M . As before, we note that $s - M^2 = 2E^2$ and $t = 4E^2 \sin^2(\theta/2)$ so we can substitute

$$\frac{d\sigma}{d\Omega} = \frac{\alpha^2}{4W} \frac{2E^2}{16E^4 \sin^4(\theta/2)}, \quad (\text{B.18})$$

which is our desired cross section. We observe the leading behavior of this scattering (for $\theta \ll 1$)

$$\frac{d\sigma}{d\Omega} \propto \frac{1}{\theta^4}. \quad (\text{B.19})$$

Derive Completeness Relation (i.e. Sum Over Spins)

Since our QED field must satisfy the Dirac Equation in momentum space, we know

$$(\not{p} - m)u(p) = 0, \quad (\text{B.20})$$

where $\not{p} = \gamma^\mu p_\mu$ and $p^\mu = (m, p^i)$ for $i = 1, 2, 3$ and where we set $c = 1$. Due to Lorentz invariance and basis independence [29], we can evaluate the above equation in the rest frame in a convenient basis, which will tell us about the general cases as well.

In the rest frame $p^\mu = (m, 0)$, so the Dirac Equation becomes $(\gamma^0 - 1)u = 0$ leading to two independent spinors

$$\begin{pmatrix} 1 \\ 0 \\ 0 \\ 0 \end{pmatrix} \text{ and } \begin{pmatrix} 0 \\ 1 \\ 0 \\ 0 \end{pmatrix}, \quad (\text{B.21})$$

which we associate with positive and negative spin respectively.

Then, using $\bar{u} \equiv u^\dagger \gamma^0$, we find that the \bar{u} are just the corresponding row vectors. Thus, the normalized spinors obey $\bar{u}(p)u(p) = 1$. Restoring the spin labels, we can now sum over all possible spin as follows

$$\begin{aligned}
\sum_s u^{(s)}(p)\bar{u}^{(s)}(p) &= \begin{pmatrix} 1 \\ 0 \\ 0 \\ 0 \end{pmatrix} \begin{pmatrix} 1 & 0 & 0 & 0 \end{pmatrix} + \begin{pmatrix} 0 \\ 1 \\ 0 \\ 0 \end{pmatrix} \begin{pmatrix} 0 & 1 & 0 & 0 \end{pmatrix} \\
&= \begin{pmatrix} 1 & 0 & 0 & 0 \\ 0 & 1 & 0 & 0 \\ 0 & 0 & 0 & 0 \\ 0 & 0 & 0 & 0 \end{pmatrix} = \begin{pmatrix} I & 0 \\ 0 & 0 \end{pmatrix} = \frac{1}{2}(\gamma^0 + 1), \quad (\text{B.22})
\end{aligned}$$

Now, by invoking Lorentz invariance (i.e. we move out of the rest frame) and basis independence, we write our completeness relation

$$\sum_s u^{(s)}(p)\bar{u}^{(s)}(p) = \frac{1}{2m}(\gamma^\mu p + m) = (\not{p} + m), \quad (\text{B.23})$$

where we temporarily ignore the normalization factor $1/(2m)$. This can easily be restored as needed [29].

Appendix C

Form Factors

Scattering on Earth

In Chapter 5, we considered a photon being scattered by a large astronomical target, represented by very heavy scalar particle. To make our predictions more precise, we may introduce a form factor, where we can approximate the target as a uniform, spherically symmetric sphere. The appropriate mass distribution is given as a step function

$$\rho(x) = \begin{cases} \frac{m}{\frac{4}{3}\pi r} & \text{if } r \leq R \\ 0 & \text{if } r > R \end{cases}, \quad (\text{C.1})$$

where R and m are the radius and the mass of the target. The formula for this simple form factor is given by

$$F(q) = \int e^{iqx} \rho(x) dx^3, \quad (\text{C.2})$$

and calculating this integral gives

$$F(q) = \frac{3m}{qR} \left(\frac{\sin(qR)}{(qR)^2} - \frac{\cos(qR)}{(qR)} \right). \quad (\text{C.3})$$

Plugging in $K_1 - K_2$ for momentum transfer q and 6.378×10^6 m for the radius, we get an appropriate form factor that we can use to improve our results above.

Appendix D

Additional Monte-Carlo Tests and Results

Test of Scattering Geometry

Tables D.1-D.4 record the final coordinates of a unit vector which undergoes basic rotations (from the initial state along the z axis) corresponding to various emission and scattering angles, as discussed in Chapter 4. These tables were constructed as a cross check of the rotation matrices used in our simulation. As in Chapter 4, (θ_0, ϕ_0) denotes initial altitudal and azimuthal angles (corresponding to emission) while (θ, ϕ) denotes a rotation from the initial trajectory (corresponding to scattering). Tables D.1-D.4 confirms that the geometry used in our simulation behaves as expected. More extensive tables and cross checks are available upon request but for brevity are omitted here.

Choosing Larger DM Masses

The figures below report the results after running the Monte-Carlo simulation, where the Dark Matter 'particle' mass is taken to be 1000 Solar Masses, which is in the upper bound region predicted by primordial black hole models of Dark Matter [51]. The photon flux, density, and all other parameters are identical to those discussed in Chapter 4.

Table D.1 Geometry Tests for Emission and Scattering Angles

| $_{-}$ | θ_0 | ϕ_0 | θ | ϕ | x | y | z |
|--------|------------|----------|----------|--------|-----|-----|-----|
| 0 | 0.0pi | 0.0pi | 0.0pi | 0.0pi | 0 | 0 | 1 |
| 1 | 0.0pi | 0.0pi | 0.0pi | 0.5pi | 0 | 0 | 1 |
| 2 | 0.0pi | 0.0pi | 0.0pi | 1.0pi | 0 | 0 | 1 |
| 3 | 0.0pi | 0.0pi | 0.0pi | 1.5pi | 0 | 0 | 1 |
| 4 | 0.0pi | 0.0pi | 0.5pi | 0.0pi | 1 | 0 | 0 |
| 5 | 0.0pi | 0.0pi | 0.5pi | 0.5pi | 0 | 1 | 0 |
| 6 | 0.0pi | 0.0pi | 0.5pi | 1.0pi | -1 | 0 | 0 |
| 7 | 0.0pi | 0.0pi | 0.5pi | 1.5pi | 0 | -1 | 0 |
| 8 | 0.0pi | 0.0pi | 1.0pi | 0.0pi | 0 | 0 | -1 |
| 9 | 0.0pi | 0.0pi | 1.0pi | 0.5pi | 0 | 0 | -1 |
| 10 | 0.0pi | 0.0pi | 1.0pi | 1.0pi | 0 | 0 | -1 |
| 11 | 0.0pi | 0.0pi | 1.0pi | 1.5pi | 0 | 0 | -1 |
| 12 | 0.0pi | 0.5pi | 0.0pi | 0.0pi | 0 | 0 | 1 |
| 13 | 0.0pi | 0.5pi | 0.0pi | 0.5pi | 0 | 0 | 1 |
| 14 | 0.0pi | 0.5pi | 0.0pi | 1.0pi | 0 | 0 | 1 |
| 15 | 0.0pi | 0.5pi | 0.0pi | 1.5pi | 0 | 0 | 1 |
| 16 | 0.0pi | 0.5pi | 0.5pi | 0.0pi | 0 | 1 | 0 |
| 17 | 0.0pi | 0.5pi | 0.5pi | 0.5pi | -1 | 0 | 0 |
| 18 | 0.0pi | 0.5pi | 0.5pi | 1.0pi | 0 | -1 | 0 |
| 19 | 0.0pi | 0.5pi | 0.5pi | 1.5pi | 1 | 0 | 0 |
| 20 | 0.0pi | 0.5pi | 1.0pi | 0.0pi | 0 | 0 | -1 |
| 21 | 0.0pi | 0.5pi | 1.0pi | 0.5pi | 0 | 0 | -1 |
| 22 | 0.0pi | 0.5pi | 1.0pi | 1.0pi | 0 | 0 | -1 |
| 23 | 0.0pi | 0.5pi | 1.0pi | 1.5pi | 0 | 0 | -1 |
| 24 | 0.0pi | 1.0pi | 0.0pi | 0.0pi | 0 | 0 | 1 |
| 25 | 0.0pi | 1.0pi | 0.0pi | 0.5pi | 0 | 0 | 1 |
| 26 | 0.0pi | 1.0pi | 0.0pi | 1.0pi | 0 | 0 | 1 |
| 27 | 0.0pi | 1.0pi | 0.0pi | 1.5pi | 0 | 0 | 1 |
| 28 | 0.0pi | 1.0pi | 0.5pi | 0.0pi | -1 | 0 | 0 |
| 29 | 0.0pi | 1.0pi | 0.5pi | 0.5pi | 0 | -1 | 0 |
| 30 | 0.0pi | 1.0pi | 0.5pi | 1.0pi | 1 | 0 | 0 |
| 31 | 0.0pi | 1.0pi | 0.5pi | 1.5pi | 0 | 1 | 0 |
| 32 | 0.0pi | 1.0pi | 1.0pi | 0.0pi | 0 | 0 | -1 |
| 33 | 0.0pi | 1.0pi | 1.0pi | 0.5pi | 0 | 0 | -1 |
| 34 | 0.0pi | 1.0pi | 1.0pi | 1.0pi | 0 | 0 | -1 |
| 35 | 0.0pi | 1.0pi | 1.0pi | 1.5pi | 0 | 0 | -1 |
| 36 | 0.0pi | 1.5pi | 0.0pi | 0.0pi | 0 | 0 | 1 |
| 37 | 0.0pi | 1.5pi | 0.0pi | 0.5pi | 0 | 0 | 1 |
| 38 | 0.0pi | 1.5pi | 0.0pi | 1.0pi | 0 | 0 | 1 |
| 39 | 0.0pi | 1.5pi | 0.0pi | 1.5pi | 0 | 0 | 1 |
| 40 | 0.0pi | 1.5pi | 0.5pi | 0.0pi | 0 | -1 | 0 |

Table D.2 Geometry Tests for Emission and Scattering Angles Cont'd

| $_$ | θ_0 | ϕ_0 | θ | ϕ | x | y | z |
|-----|------------|----------|----------|--------|-----|-----|-----|
| 41 | 0.0pi | 1.5pi | 0.5pi | 0.5pi | 1 | 0 | 0 |
| 42 | 0.0pi | 1.5pi | 0.5pi | 1.0pi | 0 | 1 | 0 |
| 43 | 0.0pi | 1.5pi | 0.5pi | 1.5pi | -1 | 0 | 0 |
| 44 | 0.0pi | 1.5pi | 1.0pi | 0.0pi | 0 | 0 | -1 |
| 45 | 0.0pi | 1.5pi | 1.0pi | 0.5pi | 0 | 0 | -1 |
| 46 | 0.0pi | 1.5pi | 1.0pi | 1.0pi | 0 | 0 | -1 |
| 47 | 0.0pi | 1.5pi | 1.0pi | 1.5pi | 0 | 0 | -1 |
| 48 | 0.5pi | 0.0pi | 0.0pi | 0.0pi | 1 | 0 | 0 |
| 49 | 0.5pi | 0.0pi | 0.0pi | 0.5pi | 1 | 0 | 0 |
| 50 | 0.5pi | 0.0pi | 0.0pi | 1.0pi | 1 | 0 | 0 |
| 51 | 0.5pi | 0.0pi | 0.0pi | 1.5pi | 1 | 0 | 0 |
| 52 | 0.5pi | 0.0pi | 0.5pi | 0.0pi | 0 | 0 | -1 |
| 53 | 0.5pi | 0.0pi | 0.5pi | 0.5pi | 0 | 1 | 0 |
| 54 | 0.5pi | 0.0pi | 0.5pi | 1.0pi | 0 | 0 | 1 |
| 55 | 0.5pi | 0.0pi | 0.5pi | 1.5pi | 0 | -1 | 0 |
| 56 | 0.5pi | 0.0pi | 1.0pi | 0.0pi | -1 | 0 | 0 |
| 57 | 0.5pi | 0.0pi | 1.0pi | 0.5pi | -1 | 0 | 0 |
| 58 | 0.5pi | 0.0pi | 1.0pi | 1.0pi | -1 | 0 | 0 |
| 59 | 0.5pi | 0.0pi | 1.0pi | 1.5pi | -1 | 0 | 0 |
| 60 | 0.5pi | 0.5pi | 0.0pi | 0.0pi | 0 | 1 | 0 |
| 61 | 0.5pi | 0.5pi | 0.0pi | 0.5pi | 0 | 1 | 0 |
| 62 | 0.5pi | 0.5pi | 0.0pi | 1.0pi | 0 | 1 | 0 |
| 63 | 0.5pi | 0.5pi | 0.0pi | 1.5pi | 0 | 1 | 0 |
| 64 | 0.5pi | 0.5pi | 0.5pi | 0.0pi | 0 | 0 | -1 |
| 65 | 0.5pi | 0.5pi | 0.5pi | 0.5pi | -1 | 0 | 0 |
| 66 | 0.5pi | 0.5pi | 0.5pi | 1.0pi | 0 | 0 | 1 |
| 67 | 0.5pi | 0.5pi | 0.5pi | 1.5pi | 1 | 0 | 0 |
| 68 | 0.5pi | 0.5pi | 1.0pi | 0.0pi | 0 | -1 | 0 |
| 69 | 0.5pi | 0.5pi | 1.0pi | 0.5pi | 0 | -1 | 0 |
| 70 | 0.5pi | 0.5pi | 1.0pi | 1.0pi | 0 | -1 | 0 |
| 71 | 0.5pi | 0.5pi | 1.0pi | 1.5pi | 0 | -1 | 0 |
| 72 | 0.5pi | 1.0pi | 0.0pi | 0.0pi | -1 | 0 | 0 |
| 73 | 0.5pi | 1.0pi | 0.0pi | 0.5pi | -1 | 0 | 0 |
| 74 | 0.5pi | 1.0pi | 0.0pi | 1.0pi | -1 | 0 | 0 |
| 75 | 0.5pi | 1.0pi | 0.0pi | 1.5pi | -1 | 0 | 0 |
| 76 | 0.5pi | 1.0pi | 0.5pi | 0.0pi | 0 | 0 | -1 |
| 77 | 0.5pi | 1.0pi | 0.5pi | 0.5pi | 0 | -1 | 0 |
| 78 | 0.5pi | 1.0pi | 0.5pi | 1.0pi | 0 | 0 | 1 |
| 79 | 0.5pi | 1.0pi | 0.5pi | 1.5pi | 0 | 1 | 0 |
| 80 | 0.5pi | 1.0pi | 1.0pi | 0.0pi | 1 | 0 | 0 |

Table D.3 Geometry Tests for Emission and Scattering Angles Cont'd

| $_$ | θ_0 | ϕ_0 | θ | ϕ | x | y | z |
|-----|------------|----------|----------|--------|-----|-----|-----|
| 81 | 0.5pi | 1.0pi | 1.0pi | 0.5pi | 1 | 0 | 0 |
| 82 | 0.5pi | 1.0pi | 1.0pi | 1.0pi | 1 | 0 | 0 |
| 83 | 0.5pi | 1.0pi | 1.0pi | 1.5pi | 1 | 0 | 0 |
| 84 | 0.5pi | 1.5pi | 0.0pi | 0.0pi | 0 | -1 | 0 |
| 85 | 0.5pi | 1.5pi | 0.0pi | 0.5pi | 0 | -1 | 0 |
| 86 | 0.5pi | 1.5pi | 0.0pi | 1.0pi | 0 | -1 | 0 |
| 87 | 0.5pi | 1.5pi | 0.0pi | 1.5pi | 0 | -1 | 0 |
| 88 | 0.5pi | 1.5pi | 0.5pi | 0.0pi | 0 | 0 | -1 |
| 89 | 0.5pi | 1.5pi | 0.5pi | 0.5pi | 1 | 0 | 0 |
| 90 | 0.5pi | 1.5pi | 0.5pi | 1.0pi | 0 | 0 | 1 |
| 91 | 0.5pi | 1.5pi | 0.5pi | 1.5pi | -1 | 0 | 0 |
| 92 | 0.5pi | 1.5pi | 1.0pi | 0.0pi | 0 | 1 | 0 |
| 93 | 0.5pi | 1.5pi | 1.0pi | 0.5pi | 0 | 1 | 0 |
| 94 | 0.5pi | 1.5pi | 1.0pi | 1.0pi | 0 | 1 | 0 |
| 95 | 0.5pi | 1.5pi | 1.0pi | 1.5pi | 0 | 1 | 0 |
| 96 | 1.0pi | 0.0pi | 0.0pi | 0.0pi | 0 | 0 | -1 |
| 97 | 1.0pi | 0.0pi | 0.0pi | 0.5pi | 0 | 0 | -1 |
| 98 | 1.0pi | 0.0pi | 0.0pi | 1.0pi | 0 | 0 | -1 |
| 99 | 1.0pi | 0.0pi | 0.0pi | 1.5pi | 0 | 0 | -1 |
| 100 | 1.0pi | 0.0pi | 0.5pi | 0.0pi | -1 | 0 | 0 |
| 101 | 1.0pi | 0.0pi | 0.5pi | 0.5pi | 0 | 1 | 0 |
| 102 | 1.0pi | 0.0pi | 0.5pi | 1.0pi | 1 | 0 | 0 |
| 103 | 1.0pi | 0.0pi | 0.5pi | 1.5pi | 0 | -1 | 0 |
| 104 | 1.0pi | 0.0pi | 1.0pi | 0.0pi | 0 | 0 | 1 |
| 105 | 1.0pi | 0.0pi | 1.0pi | 0.5pi | 0 | 0 | 1 |
| 106 | 1.0pi | 0.0pi | 1.0pi | 1.0pi | 0 | 0 | 1 |
| 107 | 1.0pi | 0.0pi | 1.0pi | 1.5pi | 0 | 0 | 1 |
| 108 | 1.0pi | 0.5pi | 0.0pi | 0.0pi | 0 | 0 | -1 |
| 109 | 1.0pi | 0.5pi | 0.0pi | 0.5pi | 0 | 0 | -1 |
| 110 | 1.0pi | 0.5pi | 0.0pi | 1.0pi | 0 | 0 | -1 |
| 111 | 1.0pi | 0.5pi | 0.0pi | 1.5pi | 0 | 0 | -1 |
| 112 | 1.0pi | 0.5pi | 0.5pi | 0.0pi | 0 | -1 | 0 |
| 113 | 1.0pi | 0.5pi | 0.5pi | 0.5pi | -1 | 0 | 0 |
| 114 | 1.0pi | 0.5pi | 0.5pi | 1.0pi | 0 | 1 | 0 |
| 115 | 1.0pi | 0.5pi | 0.5pi | 1.5pi | 1 | 0 | 0 |
| 116 | 1.0pi | 0.5pi | 1.0pi | 0.0pi | 0 | 0 | 1 |
| 117 | 1.0pi | 0.5pi | 1.0pi | 0.5pi | 0 | 0 | 1 |
| 118 | 1.0pi | 0.5pi | 1.0pi | 1.0pi | 0 | 0 | 1 |
| 119 | 1.0pi | 0.5pi | 1.0pi | 1.5pi | 0 | 0 | 1 |
| 120 | 1.0pi | 1.0pi | 0.0pi | 0.0pi | 0 | 0 | -1 |

Table D.4 Geometry Tests for Emission and Scattering Angles Cont'd

| – | θ_0 | ϕ_0 | θ | ϕ | x | y | z |
|-----|------------|----------|----------|--------|-----|-----|-----|
| 121 | 1.0pi | 1.0pi | 0.0pi | 0.5pi | 0 | 0 | -1 |
| 122 | 1.0pi | 1.0pi | 0.0pi | 1.0pi | 0 | 0 | -1 |
| 123 | 1.0pi | 1.0pi | 0.0pi | 1.5pi | 0 | 0 | -1 |
| 124 | 1.0pi | 1.0pi | 0.5pi | 0.0pi | 1 | 0 | 0 |
| 125 | 1.0pi | 1.0pi | 0.5pi | 0.5pi | 0 | -1 | 0 |
| 126 | 1.0pi | 1.0pi | 0.5pi | 1.0pi | -1 | 0 | 0 |
| 127 | 1.0pi | 1.0pi | 0.5pi | 1.5pi | 0 | 1 | 0 |
| 128 | 1.0pi | 1.0pi | 1.0pi | 0.0pi | 0 | 0 | 1 |
| 129 | 1.0pi | 1.0pi | 1.0pi | 0.5pi | 0 | 0 | 1 |
| 130 | 1.0pi | 1.0pi | 1.0pi | 1.0pi | 0 | 0 | 1 |
| 131 | 1.0pi | 1.0pi | 1.0pi | 1.5pi | 0 | 0 | 1 |
| 132 | 1.0pi | 1.5pi | 0.0pi | 0.0pi | 0 | 0 | -1 |
| 133 | 1.0pi | 1.5pi | 0.0pi | 0.5pi | 0 | 0 | -1 |
| 134 | 1.0pi | 1.5pi | 0.0pi | 1.0pi | 0 | 0 | -1 |
| 135 | 1.0pi | 1.5pi | 0.0pi | 1.5pi | 0 | 0 | -1 |
| 136 | 1.0pi | 1.5pi | 0.5pi | 0.0pi | 0 | 1 | 0 |
| 137 | 1.0pi | 1.5pi | 0.5pi | 0.5pi | 1 | 0 | 0 |
| 138 | 1.0pi | 1.5pi | 0.5pi | 1.0pi | 0 | -1 | 0 |
| 139 | 1.0pi | 1.5pi | 0.5pi | 1.5pi | -1 | 0 | 0 |
| 140 | 1.0pi | 1.5pi | 1.0pi | 0.0pi | 0 | 0 | 1 |
| 141 | 1.0pi | 1.5pi | 1.0pi | 0.5pi | 0 | 0 | 1 |
| 142 | 1.0pi | 1.5pi | 1.0pi | 1.0pi | 0 | 0 | 1 |
| 143 | 1.0pi | 1.5pi | 1.0pi | 1.5pi | 0 | 0 | 1 |

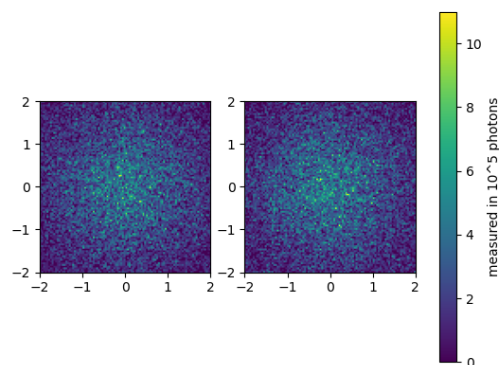


Fig. D.1 Photon hits near Earth (a) and (b) correspond to the two states of linear polarization.

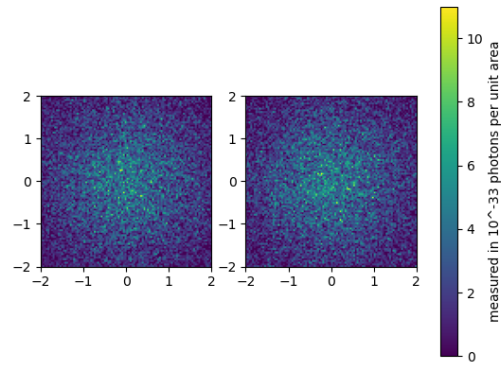


Fig. D.2 Difference between photon hits of either polarization per unit area.

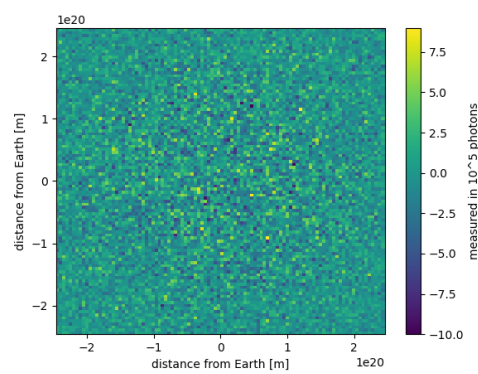


Fig. D.3 Difference between photon hits of either polarization.